

EFC++: Elastic Feature Consolidation with Prototype Re-balancing for Cold Start Exemplar-free Incremental Learning

Simone Magistri*, Tomaso Trinci*, Albin Soutif–Cormerais, Joost van de Weijer, Andrew D. Bagdanov

Abstract—Exemplar-Free Class Incremental Learning (EFCIL) aims to learn from a sequence of tasks without having access to previous task data. In this paper, we consider the challenging Cold Start scenario in which insufficient data is available in the first task to learn a high-quality backbone. This is especially challenging for EFCIL since it requires high plasticity, resulting in feature drift which is difficult to compensate for in the exemplar-free setting. To address this problem, we propose an effective approach to consolidate feature representations by regularizing drift in directions highly relevant to previous tasks and employs prototypes to reduce task-recency bias. Our approach, which we call Elastic Feature Consolidation++ (EFC++) exploits a tractable second-order approximation of feature drift based on a proposed Empirical Feature Matrix (EFM). The EFM induces a pseudo-metric in feature space which we use to regularize feature drift in important directions and to update Gaussian prototypes. In addition, we introduce a post-training prototype re-balancing phase that updates classifiers to compensate for feature drift. Experimental results on CIFAR-100, Tiny-ImageNet, ImageNet-Subset, ImageNet-1K and DomainNet demonstrate that EFC++ is better able to learn new tasks by maintaining model plasticity and significantly outperform the state-of-the-art.[†]

Index Terms—Class-Incremental Learning, Continual Learning, Catastrophic Forgetting, Computer Vision.

I. INTRODUCTION

IN recent years, Deep Neural Networks (DNNs) like Convolutional Neural Networks [1] and Vision Transformers [2] have achieved remarkable success for a large variety of artificial intelligence applications but have also introduced additional training complexities. The standard supervised learning paradigm requires massive datasets for robust generalization [3], and collecting large amounts of labeled data in a single session can

be impractical due to time and cost constraints. Moreover, in real-world applications like autonomous driving [4], multimedia forensics [5], healthcare [6] or remote-sensing [7], data are not stationary, often necessitating the adaptation of DNNs to new data and tasks.

Updating models with new data is challenging due to the phenomenon known as *catastrophic forgetting* [8], [9]: unlike the human brain, when a DNN learns new tasks it quickly forgets how to perform the previously-learned ones. This phenomenon is attributed to the high *plasticity* of neural networks when learning new tasks, which invariably updates parameters crucial to previous tasks in order to accommodate the new one [10]. The objective of Class Incremental Learning (CIL) is to integrate new classification tasks into existing models as they arise, without needing to reuse all data from previously seen classes, thereby striking a better balance between performance and training efficiency [11]. To achieve this, CIL focuses on enhancing the stability of network learning to preserve knowledge from previously seen classes and reduce the risk of catastrophic forgetting. However, increasing stability alone is insufficient, as an overly stable network may struggle to adapt to new classes, thereby inhibiting plasticity. Consequently, the key challenge in CIL is to find the right equilibrium between stability and plasticity during network training. Striking this balance is often referred to as the *stability-plasticity dilemma* [12], [13].

Relying solely on data from the current task to mitigate catastrophic forgetting is challenging because the final deep representation and classifier tend to be highly biased towards the most recent task (a phenomenon known as *task-recency bias*). Additionally, the final classifier is never trained to distinguish among all the encountered classes (a phenomenon called *inter-task confusion* [14]). To address this, many recent CIL approaches, known as Exemplar-based Class Incremental Learning (EBCIL) methods, store samples from previous tasks (e.g., 20 per class) as exemplars and replay them while learning new tasks [15], [16], [17]. While effective, these methods require additional storage and computational resources, which can scale with the number of tasks. Furthermore, storing samples can pose significant privacy issues, as it may not always be feasible to retain such data due to privacy concerns. For these reasons, in this paper we focus on the more general and challenging incremental learning setting without exemplars, a paradigm known as Exemplar-free Class Incremental Learning (EFCIL).

Elastic Weight Consolidation (EWC) is a pioneering work

Manuscript Submitted on July, 2024. This work was supported by funding by the European Commission Horizon 2020 grant #951911 (AI4Media), TED2021-132513B-I00 and PID2022-143257NB-I00 funded by MCIN/AEI/ 10.13039/501100011033, by the Italian national Cluster Project CTN01_00034_23154 “Social Museum Smart Tourism”, by the European Union project NextGenerationEU/PRTR, and by the Spanish Development Fund FEDER. [†] Code to reproduce the results of EFC++ will be released upon acceptance of this work, code for EFC is available at https://github.com/simomagi/elastic_feature_consolidation.git

* Equal Contribution

Simone Magistri and Tomaso Trinci are with the Media Integration and Communication Center, 50134 Florence, Italy and the Global Optimization Laboratory, 50136 Florence, Italy.

E-mail: {simone.magistri, tomaso.trinci}@unifi.it

Albin–Soutif Cormerais and Joost van de Weijer are with LAMP Team, Computer Vision Center, 08036 Barcelona, Spain.

E-mail: {albin, joost}@cvc.uab.es.

Andrew D. Bagdanov is with the Media Integration and Communication Center, 50134 Florence, Italy.

E-mail: andrew.bagdanov@unifi.it

in EFCIL [10]. EWC addresses catastrophic forgetting via weight regularization. EWC is an elegant approach based on a Laplace approximation of the previous task posterior. When training on a new task, an approximate Fisher Information Matrix is used to regularize parameter drift to prevent the optimization from harming parameters important for previous tasks, while simultaneously increasing plasticity to learn new tasks. Since computing the full Fisher Information Matrix is intractable (its size is quadratic in the number of network parameters), EWC uses a diagonal approximation of the matrix. This approximation is an aggressive simplification compared to the full matrix and results in a significant performance drop [18], [19].

Given the difficulties in regularizing network weights, recent EFCIL methods rely on the more tractable functional regularization paradigm which mitigates network activation drift during incremental learning. Feature distillation, consisting in regularizing feature space drift via ℓ_2 regularization, is a central component in recent state-of-the-art EFCIL approaches [20], [21], [22], [23], [24]. Feature distillation is often combined with class prototypes, either learned [23] or based on class means [21], to perform pseudo-rehearsal of feature from previous tasks in order to reduce task-recency bias and inter-task confusion phenomenon. Prototypes – differently from exemplars – offer an efficient and privacy-preserving way to mitigate forgetting.

While feature distillation effectively mitigates forgetting through increased stability, it does so at the cost of reduced plasticity for learning new tasks [25]. A similar emphasis on stability is also observed in other recent EFCIL methods that freeze the backbone after the first task and focus solely on incrementally learning the classifier [26], [27]. This emphasis on stability largely stems from the standard evaluation setting for EFCIL methods [22], [21], [23], [26], [27]. In this setting, called the *Warm Start* scenario, the first task includes a large fraction of the total classes, typically 40% or 50%, making stability more critical than plasticity. Since a high-quality feature extractor is learned in the first task, it improves generalization in subsequent tasks. However, when the initial task is smaller, an incremental learning method must increase plasticity to compensate for the lack of a strong initial feature extractor, requiring substantial updates to the backbone in order to effectively learn new tasks.

In Figure 1 we give an empirical analysis via linear probing to demonstrate the importance of plasticity in EFCIL for different initial task sizes. These results show that for smaller initial task sizes (e.g. $C_0 = 10$), the plasticity potential Δ – defined as the maximum performance gain which can be obtained with a plastic versus a frozen backbone – is highest. This reflects the greater need for feature adaptation in later incremental learning stages, as a weaker initial backbone demands more flexibility to incorporate new knowledge.

In this paper we examine EFCIL in the more challenging *Cold Start* scenario in which the first task is insufficiently large to learn a high-quality backbone and methods must be plastic and adapt their backbone to new tasks. Although this scenario has been explored in the EFCIL literature [17], [16], it is rarely addressed in EFCIL due to several challenges.

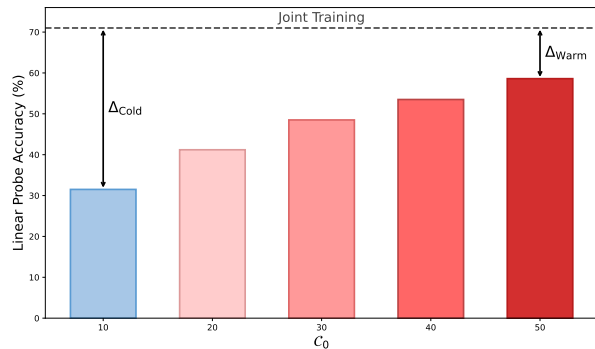


Fig. 1. Plasticity potential in Cold and Warm Start. We train a ResNet-18 on C_0 classes of CIFAR-100 for $C_0 = 10, 20, \dots, 50$, and evaluate feature quality via linear probing [28] on all 100 classes. The plasticity potential Δ , defined as the maximum performance gain which can be obtained with a plastic versus a frozen backbone, is quantified as the performance gap between Joint Training and a model frozen on a subset of classes. Note that Δ_{Cold} (the *Cold Start* scenario) is significantly larger than Δ_{Warm} (the *Warm Start* case). This is due to the inability to learn a strong feature extractor on only C_0 classes and hence greater plasticity is required to incrementally learn new classes. Freezing the backbone in such settings limits adaptability and ultimately constrains performance on subsequent tasks.

In Cold Start scenarios, representations are more prone to change than in Warm Start, making it difficult to control drift without compromising plasticity – especially when there are no exemplars to rely on. Additionally, using a strict regularizer, like feature distillation or freezing the backbone, prevents the network from adapting to new data. Therefore, an alternative to feature distillation is necessary, and an exemplar-free mechanism is needed to adapt previous-task classifiers to the evolving backbone.

To specifically address the challenges of Cold Start, we propose a novel EFCIL approach, *Elastic Feature Consolidation with Prototype Re-balancing*, hereafter referred to as EFC++, which builds upon and enhances our previously published method EFC [29]. EFC++ regularizes variations along the directions in the *feature space* that are most critical for past tasks while allowing more plasticity in other directions. To identify these directions, we derive a pseudo-metric in feature space, induced by a matrix we coined the *Empirical Feature Matrix* (EFM). Unlike the Fisher Information Matrix, the EFM can be easily computed and stored since its size depends only on the feature space dimensionality and not on the number of model parameters. In addition, EFC++ decouples backbone training from classifier learning through a *prototype re-balancing* phase, allowing significant improvements over EFC in Cold Start settings by more effectively leveraging prototypes and managing the plasticity introduced by the EFM. A visual overview EFC++ is given in Figure 2.

EFC++ improves upon EFC and excels in Cold Start EFCIL across multiple benchmarks, further widening the gap with respect to the state of the art in EFCIL without incurring significant additional computational overhead. We also expand the scope of our comparative performance analysis to include recent state-of-the-art EFCIL methods [27], [30], [31] and test on broader range of benchmarks from small-scale (CIFAR-100, Tiny ImageNet, and ImageNet-Subset), to large-scale (ImageNet-1K), and a domain- and class-incremental

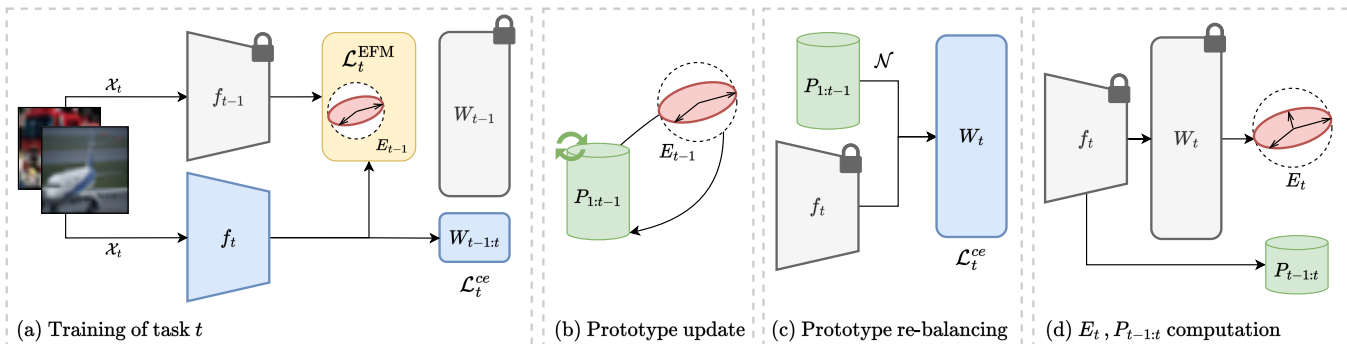


Fig. 2. Elastic Feature Consolidation with Prototype re-balancing (EFC++). (a) EFC++ leverages the Empirical Feature Matrix (EFM) to mitigate drift in feature representations by identifying important directions for previous tasks to reduce forgetting while enhancing plasticity for learning new tasks (Section III-C). In this phase, the feature extractor f_t and the current task classifier with weights $W_{t-1:t}$ are trained with EFM regularization and cross-entropy loss (Section IV-B). (b) After training, EFC++ uses the EFM to update the prototypes of previous task classes based on the drift induced by the most recent task (Section IV-C). (c) EFC++ uses Gaussian prototypes, together current task features, for training previous and current task classifiers with weights $W_t = [W_{t-1}, W_{t-1:t}]$ via a prototype re-balancing phase (Section IV-B). (d) Before training on the next task, the new EFM and the prototypes of the current task classes are computed.

learning setting (DomainNet [32]) to assess performance under substantial domain shifts. Through ablation studies, we demonstrate how the EFM regularizer in EFC++ achieves a better stability-plasticity trade-off and overall performance compared to other popular incremental learning regularizers. Finally, we compare representation drift in Warm Start and Cold Start scenarios, provide a spectral analysis of the EFM in Cold Start, examine the impact of hyperparameters, and discuss the limitations of EFC++.

The paper is organized as follows. In the next section, we review the literature on EFCIL most related to our contributions. Then, in Section III we introduce the Empirical Feature Matrix (EFM) and discuss its role in feature space regularization. Section IV details the training procedure of EFC++, which includes training the feature extractor with the EFM regularizer and refining the final classifier through prototype re-balancing. We also explain how we use the the EFM for prototype drift compensation. In Section V we compare EFC with EFC++ and highlight the improvements of EFC++ over EFC in Cold Start. Sections VI and VII describe our experimental setup and results which compare EFC++ with state-of-the-art EFCIL methods. In Section VIII we provide ablation studies of EFC++ along with additional analyses, including feature space drift in Warm Start and Cold Start scenarios, a spectral analysis of the Empirical Feature Matrix and its impact on hyperparameter selection, storage and computational considerations, and a discussion of its limitations. Finally, we conclude in Section IX with a discussion of our contributions and some indications of potential future research lines.

II. RELATED WORK

The primary goal of incremental learning is to continuously acquire new knowledge from a non-stationary data stream while mitigating the issue of catastrophic forgetting. In this study, we concentrate on **offline class-incremental** learning problems. Class-incremental scenario is distinguished from task-incremental one in that no task information is available at test time and thus is more challenging [33], [34]. Offline incremental learning allows multiple passes on task datasets during training, while online incremental learning considers

continuous data streams in which each sample is accessed just once during training [35], [36], [37], [38], [39].

A significant portion of offline class incremental learning research focuses on Exemplar-Based Class Incremental Learning (EBCIL) approaches. These methods integrate regularization techniques with replay mechanisms, utilizing a memory of previous class samples that are replayed during the learning of new tasks. iCaRL [40] employs Nearest Mean Classification (NMC) along with exemplars and utilizes Knowledge Distillation [41] during training to mitigate forgetting. Techniques like BiC [42] and IL2M [43] correct network outputs using exemplars to mitigate inter-task confusion and task-recency bias. DER++[44] and its recent variant X-DER[45] replay both logits and ground-truth labels via self-distillation on exemplars. LUCIR [46], PODNet [25], and AFC [15] combine cosine normalization and distillation losses with exemplars to reduce forgetting. Another category of exemplar-based approaches focuses on expanding sub-network structures across incremental steps. AANET [47] adds two residual blocks to mask layers, balancing stability and plasticity. DER [16] trains a single backbone for each incremental task, while MEMO [17] shares generalized residual blocks and extends specialized blocks for new tasks to improve performance and efficiency. The main drawbacks of exemplar-based approaches are the lack of privacy preservation and high computational and storage costs, especially when using a growing memory buffer or when dynamic expanding the network.

Exemplar-free Class Incremental Learning (EFCIL) mitigating catastrophic forgetting without rely upon exemplars from previous tasks. These approaches are less common in class-incremental learning. Early works such as EWC [10], [48], Rwalk [49], MAS [50], SI [51], focused on calculating importance scores for all neural network weights. These importance scores are then used to regularize the network training, ensuring that the current learned weights do not update parameters crucial to the performance of previous task. Recently Benzing et al. [52] show that the importance score compute by the aforementioned methods approximate the Fisher Information Matrix.

Another research direction, exemplified by methods like

Learning without Forgetting (LwF) [53] and Less-forgetful Learning (LFL) [54], utilizes functional regularization techniques such as knowledge and feature distillation respectively. These methods constrain network activations to mirror those of a previously trained network, a strategy shown to surpass weight regularization in performance [14]. Most recent functional regularization approaches use feature distillation [55], [24], [21], [22], [23], [20], or even freeze the feature extractor after the first task [26], [27], [56], greatly reducing the plasticity of the network. For this reason, they predominantly consider Warm Start scenarios in which the first task is much larger than the others, so that reducing plasticity after the first task has less impact on the performance.

On top of this decrease in plasticity, merely using functional regularization is not enough to learn new boundaries between classes from previous tasks and classes from new ones. To address this issue without using exemplars, a line of research employs generative models [20], [57], [58], [31], [59], [30], [60] to create synthetic samples from previous tasks and replay them while learning the new tasks. However, training generative models concurrently with new tasks is inefficient, and these models are prone to forgetting [21]. Consequently, recent approaches combine regularization with *prototype rehearsal* [21], [55]. Prototypes are feature space statistics (typically class means) used to reinforce the boundaries of previous-task classes without the need to preserve exemplars. PASS [21] and IL2A [55] propose the integration of gaussian prototypes and self-supervised learning to learn transferable features for future tasks. Evanescent [23] learns and updates prototype representations during incremental learning. SSRE [22] replay over-sampled prototypes during the current task training and employs a strategy to reorganize network structure to transfer invariant knowledge across the tasks. FeTrIL [26] fixes the feature extractor after the initial large task and generates pseudo-samples, combining prototypes with current task features, to train a linear model that discriminates all observed classes. Similarly, FeCAM [27] freezes the backbone after the first task, but employs prototypes and the corresponding class covariances to compute the Mahalanobis Distance at inference time to distinguish samples belonging to classes in different tasks.

In this study, we introduce an EFCIL method that incorporates both functional regularization and prototype rehearsal. Unlike many existing state-of-the-art approaches, our method enhances the plasticity within incremental learning processes. We demonstrate that this increased plasticity benefits *Cold Start* incremental learning scenarios, which begin without a large initial task and are rarely addressed by EFCIL literature.

III. FEATURE DRIFT REGULARIZATION VIA THE EMPIRICAL FEATURE MATRIX

In this section we introduce the general EFCIL framework and then derive a novel pseudo-metric in feature space, induced by a positive semi-definite matrix we call the *Empirical Feature Matrix* (EFM), used as a regularizer to control feature drift during class-incremental learning.

A. Exemplar-free Class-Incremental Learning (EFCIL)

During class-incremental learning a model \mathcal{M}_t is sequentially trained on K tasks, each characterized by a disjoint set of classes $\{\mathcal{C}_t\}_{t=1}^K$, where each \mathcal{C}_t is the set of labels associated to the task t . We denote the incremental dataset as $\mathcal{D} = \{\mathcal{X}_t, \mathcal{Y}_t\}_{t=1}^K$, where \mathcal{X}_t and \mathcal{Y}_t are, respectively, the set of samples and the set of labels for task t . The incremental model \mathcal{M}_t at task t consists of a feature extraction backbone $f(\cdot; \theta_t)$ shared across all tasks and whose parameters θ_t are updated during training, and a classifier $W_t \in \mathbb{R}^{n \times \sum_{j=1}^t |\mathcal{C}_j|}$ which grows with each new task. Let σ be the softmax activation function, the model output at task t is the composition of feature extractor and classifier:

$$\mathcal{M}_t(x; \theta_t, W_t) \equiv p(y|x; \theta_t, W_t) = \sigma(W_t^\top f(x; \theta_t)). \quad (1)$$

For notation purposes, we define $\mathbf{X} \sim \mathcal{X}_t$ as a batch of current task data with labels $\mathbf{Y} \sim \mathcal{Y}_t$, sampled from the overall dataset, and $f(\mathbf{X}; \theta_t)$ as the feature extractor output on the mini-batch. Thus, the model output at task t for the mini-batch \mathbf{X} is:

$$\mathcal{M}_t(\mathbf{X}; \theta_t, W_t) \equiv p(\mathbf{Y}|\mathbf{X}; \theta_t, W_t) = \sigma(W_t^\top f(\mathbf{X}; \theta_t)). \quad (2)$$

Directly training \mathcal{M}_t (i.e. fine-tuning) with a cross-entropy loss at each task t results in backbone drift because at task t we see no examples from previous-task classes. This progressively invalidates the previous-task classifiers and results in forgetting. In addition to the cross-entropy loss, many state-of-the-art EFCIL approaches use a regularization loss to reduce backbone drift, and a prototype loss to adapt previous-task classifiers to new features.

B. Weight Regularization and Feature Distillation

Kirckpatrick et al. [10] showed that using ℓ_2 regularization to constrain weight drift reduces forgetting but does not leave enough plasticity for learning of new tasks. Hence, they proposed Elastic Weight Consolidation (EWC), which relaxes the ℓ_2 constraint with a quadratic constraint based on a diagonal approximation of the Empirical Fisher Information Matrix (E-FIM):

$$F_t = \mathbb{E}_{x \sim \mathcal{X}_t} \left[\mathbb{E}_{y \sim p(y|x; \theta_t^*)} \left[\left(\frac{\partial \log p(y)}{\partial \theta_t^*} \right) \left(\frac{\partial \log p(y)}{\partial \theta_t^*} \right)^\top \right] \right], \quad (3)$$

where θ_t^* is the model trained after task t . The E-FIM induces a pseudo-metric in parameter space [61] encouraging parameters to stay in a low-error region for previous-task models:

$$\mathcal{L}_t^{\text{E-FIM}} := \lambda_{\text{E-FIM}} (\theta_t - \theta_{t-1}^*)^\top F_{t-1} (\theta_t - \theta_{t-1}^*). \quad (4)$$

The main limitation of approaches of this type is need for approximations of the E-FIM (e.g. a diagonal assumption). This makes the computation of the E-FIM tractable, but in practice is unrealistic since it does not consider off-diagonal entries that represent influences of interactions between weights on the log-likelihood. To overcome these limitations, more recent EFCIL approaches [21], [22] rely on feature distillation (FD), which scale better in the number of parameters:

$$\mathcal{L}_t^{\text{FD}} := \sum_{x \in \mathbf{X}} \|f(x; \theta_t) - f(x; \theta_{t-1})\|_2, \quad (5)$$

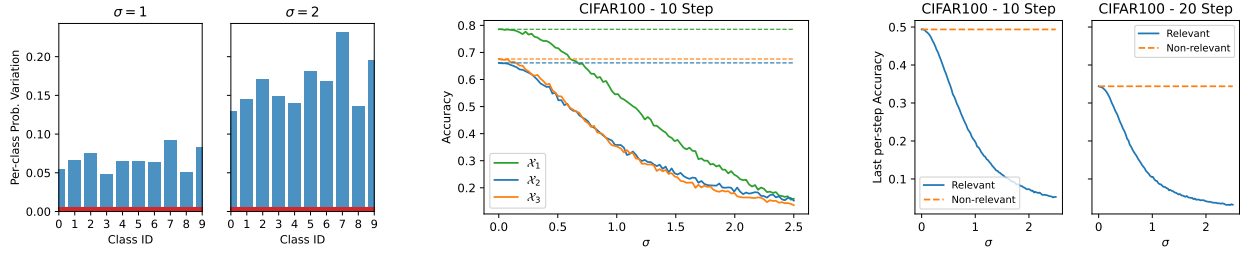


Fig. 3. The regularizing effects of E_t on the Cold Start CIFAR-100 - 10 and 20 step scenarios (see Section VI-A for details on dataset settings). **Left:** Perturbing features in the principal directions of E_1 results in significant changes in classifier outputs (in blue), while perturbations in non-principal directions leave the outputs unchanged (in red). **Middle:** If we continue incremental learning up through task 3 and perturb features from all three tasks in the principal (solid lines) and non-principal (dashed lines) directions of E_3 , we see that E_3 captures *all* important directions in feature space up through task 3. **Right:** At the end of training, we observe the same behavior: the last per-step accuracy (see Eq. 21), representing the average accuracy over all tasks after the last training session, decreases only when perturbed in directions of E_{10} or E_{20} relevant for previous tasks in the 10-step and 20-step scenarios, respectively.

where $\mathbf{X} \sim \mathcal{X}_t$.

The isotropic regularizer using the ℓ_2 distance is too harsh a constraint for learning new tasks [25]. We propose to use a pseudo-metric in *feature space*, induced by a matrix which we call the *Empirical Feature Matrix* (EFM), which constrains directions in *feature space* most important for previous tasks, while allowing more plasticity in other directions when learning new tasks. As shown in Figure 1, increasing plasticity is particularly relevant in Cold Start incremental learning since, in the initial task, a high-quality feature representation cannot be learned and methods must be plastic to adapt their backbone to new tasks.

C. The Empirical Feature Matrix

Our goal is to regularize feature drift, but we do not want to do so isotropically as in feature distillation. Instead, we draw inspiration from how the E-FIM identifies important directions in parameter space and take a similar approach in feature space (see Figure 2a).

The local and empirical feature matrices. Let $f(x; \theta_t)$ be the feature vector extracted from input $x \in \mathcal{X}_t$ from task t and $p(y) = p(y|f(x; \theta_t); W_t)$ the discrete probability distribution over all the classes seen so far. We define the *local feature matrix* as:

$$E_{f(x; \theta_t)} = \mathbb{E}_{y \sim p(y)} \left[\left(\frac{\partial \log p(y)}{\partial f(x; \theta_t)} \right) \left(\frac{\partial \log p(y)}{\partial f(x; \theta_t)} \right)^\top \right]. \quad (6)$$

The Empirical Feature Matrix (EFM) associated with task t is obtained by taking the expected value of Eq. 6 over the entire dataset at task t :

$$E_t = \mathbb{E}_{x \sim \mathcal{X}_t} [E_{f(x; \theta_t)}]. \quad (7)$$

Both $E_{f(x; \theta_t)}$ and E_t are symmetric, as they are weighted sums of symmetric matrices, and positive semi-definite. Naively computing $E_{f(x; \theta_t)}$ requires a complete forward pass and a backward pass up to the feature embedding, however we exploit an analytic formulation that avoids computing gradients:

$$E_{f(x; \theta_t)} = \mathbb{E}_{y \sim p(y)} [W_t(I_m - P)_y(W_t(I_m - P)_y)^\top], \quad (8)$$

where $m = \sum_{j=1}^t |C_j|$, I_m the identity matrix of dimension $m \times m$, and P is a matrix built from the row of softmax outputs

associated with $f(x; \theta_t)$ replicated m times (see Appendix B for a derivation).

To gain additional insight into what this matrix measures, we highlight some (information) geometry aspects of E_t . The Empirical Fisher Information Matrix provides information about the information geometry of parameter space. In particular, it can be obtained as the second derivative of the KL-divergence for small weight perturbations [62], [63]. Similarly, the Empirical Feature Matrix provides information about the information geometry of *feature space*. Since $E_{f_t(x)}$ is positive semi-definite, we can interpret it as a pseudo-metric in feature space and use it to understand which perturbations of features most affect the predicted probability:

$$\begin{aligned} & \text{KL}(p(y | f(x; \theta_t) + \delta; W_t) || p(y | f(x; \theta_t); W_t)) \\ &= \delta^\top E_{f(x; \theta_t)} \delta + \mathcal{O}(\|\delta\|^3). \end{aligned} \quad (9)$$

The Empirical Feature Matrix loss. We now have all the ingredients for our regularization loss. Let $\delta(x) = f(x; \theta_t) - f(x; \theta_{t-1})$ be the drift between the features of sample x extracted from the current model \mathcal{M}_t and the model \mathcal{M}_{t-1} trained on the previous task, then

$$\mathcal{L}_t^{\text{EFM}} := \mathbb{E}_{x \in \mathbf{X}} [\delta(x)^\top (\lambda_{\text{EFM}} E_{t-1} + \eta I) \delta(x)], \quad (10)$$

where $\mathbf{X} \sim \mathcal{X}_t$. In Eq. 10 we employ a damping term $\eta \in \mathbb{R}$ to constrain features to stay in a region where the quadratic second-order approximation of the KL-divergence of the log-likelihood in Eq. 9 remains valid [64]. However, to ensure that our regularizer does not degenerate into feature distillation, we must ensure that $\lambda_{\text{EFM}} \nu_i > \eta$, where ν_i are the non-zero eigenvalues of the EFM. Additional analysis of these constraints and the spectrum of the EFM are given in Section VIII-C.

It should be noted that the regularization in Eq. 10 does not explicitly suppress perturbations along the principal directions of E_{t-1} , but rather discourages movement along them. The term $\delta(x)^\top E_{t-1} \delta(x) = \delta(x)^\top U_{t-1} \Lambda_{t-1} U_{t-1}^\top \delta(x)$, highlights this, where U_{t-1} is the eigenvector matrix of E_{t-1} and Λ_{t-1} is the corresponding diagonal matrix of eigenvalues sorted from larger to smaller. The penalty is larger when $\delta(x)$ aligns with the eigenvectors of E_{t-1} associated with larger eigenvalues in Λ_{t-1} . Conversely, the loss is lower when $\delta(x)$ aligns with eigenvectors corresponding to smaller eigenvalues. As a result, updates are naturally biased toward directions of

lower significance since they incur a smaller penalty. The damping term $\eta\delta(x)^\top I\delta(x)$ stabilizes updates and limits drift in the directions associated with lower eigenvalues. In the next section we give empirical evidence of the effect of this elastic regularization.

The Regularizing effects of the EFM. By definition, eigenvectors of the EFM associated with strictly positive eigenvalues correspond to feature directions where perturbation most significantly impact the predictions. To empirically validate this, we perturb features along these *principal* directions and measure the variation in probability outputs.

Let $f_t = f(x; \theta_t) \in \mathbb{R}^n$ be the feature vector extracted from x , and E_t denote the EFM after training on task t . We define a perturbation vector $\varepsilon_{1:k} \in \mathbb{R}^n$, where the first k entries are sampled from a Gaussian $\mathcal{N}(0, \sigma)$, with k being the number of strictly positive eigenvalues of the spectral decomposition of E_t . The remaining $n-k$ entries are set to zero. Then, letting U_t be the matrix whose columns are the eigenvectors of E_t , we compute the perturbed features vector \tilde{f}_t as follows:

$$\tilde{f}_t = f + U_t^\top \varepsilon_{1:k}. \quad (11)$$

In Figure 3 (left), perturbing the feature space along these principal directions after training the first task, leads to a substantial variation in class probabilities. Conversely, applying the complementary perturbation $\varepsilon_{k:n}$, i.e., setting zero on the first k directions and applying Gaussian noise on the remaining $n-k$ directions, has no impact on the output. In Figure 3 (middle) we see that, after training three tasks, perturbing in the principal directions of E_3 degrades performance across all tasks, while perturbations in non-principal directions continue to have no effect on the accuracy. This shows that E_3 captures the important feature directions for all previous tasks and that regularizing drift in these directions should mitigate forgetting.

Finally, the rightmost plot in Figure 3 illustrates the per-step accuracy at the end of the training, reflecting the overall continual learning performance (see Section VI-C for a formal definition). As observed earlier, perturbing features along the principal directions of E_{10} (or E_{20}) rapidly decreases performance, while perturbations in non-principal directions have no impact on the overall accuracy. This confirms that this behavior remains consistent across all tasks.

IV. ELASTIC FEATURE CONSOLIDATION WITH PROTOTYPE RE-BALANCING

In this section, we first describe prototype rehearsal in EFCIL. Next, we introduce our training strategy that decouples feature extractor learning (with the EFM regularizer) from final intra-task classifier training via a *prototype re-balancing* phase. We then show how the Empirical Feature Matrix E_t can be used for prototype drift compensation, and finally, we present our overall methodology.

A. Prototype Rehearsal for EFCIL

EFCIL suffers from the fact that the final classifier is never jointly trained on the all seen classes. At each task t , the classifier W_{t-1} is extended to include $|\mathcal{C}_t|$ new outputs,

resulting in a classifier with weights $W_t = [W_{t-1}, W_{t-1:t}]$. Thus, if classifier W_t is only trained on samples from the current classes \mathcal{C}_t , it becomes incapable of discriminating classes from previous tasks, leading to *inter-task confusion*. Additionally, the classifier is biased towards the newest classes, resulting in *task-recency bias* [14], [42].

A common *exemplar-free* solution is to replay only *prototypes* of previous classes [20], [21], [22], [23], [26], [55]. At the end of task $t-1$, the prototypes p_{t-1}^c are computed as the class means of deep features, and the set of prototypes $\mathcal{P}_{1:t-1}$ is stored. During training for the next task, while the feature extractor is updated, the classifier is trained using a classification loss on prototypes, perturbed with Gaussian noise, along with the current task data. This strategy enables the classifier to distinguish classes across different tasks, mitigating inter-task confusion and task-recency bias problems [20], [21], [22], [23], [55].

However, most of these prototype-rehearsal strategies rely on a strong feature distillation regularizer (see Eq. 5) to be effective, which inherently restricts plasticity. As a result, they are not suitable for Cold Start scenarios, where high plasticity is crucial to learning new tasks [29]. To address this limitation, we propose to decouple the feature-extractor learning phase, incorporating our EFM regularizer (Eq. 10), from the prototype rehearsal phase. Specifically, we introduce a prototype re-balancing training strategy, applied after training the feature extractor, which leverages both prototypes and current task data. This approach mitigates inter-task confusion and task-recency bias while preserving high plasticity, making it particularly well-suited for Cold Start scenarios.

B. Prototype Re-balancing Training

We decouple the regularization phase via the Empirical Feature Matrix and the phase of learning the final inter-task classifier. In the first stage (Figure 2a), we train *the feature extractor* and *the current task classifier* with the following training loss:

$$\mathcal{L}_t^{\text{train}} := \mathcal{L}_t^{\text{EFM}} + \mathcal{L}_t^{\text{ce}}(f(\mathbf{X}, \theta_t); W_{t-1:t}). \quad (12)$$

where $\mathbf{X} \sim \mathcal{X}_t$ and $W_{t-1:t}$ represents the weights of the classifier associated with the latest classes. The cross-entropy loss is evaluated only on the current task classes, and is used to learn the features of the current task. $\mathcal{L}_t^{\text{EFM}}$ is the regularization loss based on Empirical Feature Matrix (see Eq. (10)) and is used to mitigate feature drift in the relevant directions for the previous task while allowing plasticity in the other directions.

During the post-training stage, which we call *prototype re-balancing* phase (Figure 2c), we train all classifiers up to the current task using prototypes and freezing the feature extractor:

$$\mathcal{L}_t^{\text{post-train}} := \mathcal{L}_t^{\text{ce}}(\tilde{\mathbf{P}} \cup f(\mathbf{X}, \theta_t^*); W_t), \quad (13)$$

where θ_t^* represents the frozen weights of the feature extractor and $W_t = [W_{t-1}, W_{t-1:t}]$ represents the learnable weights of the final classifier for the previous and current task classes. In this phase, we construct mini-batches by mixing prototypes, $\tilde{p}_{t-1}^c \in \tilde{\mathbf{P}}$, sampled from a Gaussian distribution $\mathcal{N}(p_{t-1}^c, \Sigma^c)$, with current task representations obtained from the frozen

feature extractor $f(\mathbf{X}, \theta_t^*)$. The covariance matrix Σ^c represents the feature covariance of class c , computed in the task where class c was introduced. Prototypes and current task data are uniformly sampled from all encountered classes to ensure balanced representation. Since the goal is to enable the final classifier to distinguish among classes from different tasks, the cross-entropy loss is evaluated over all encountered classes.

However, employing fixed prototypes p_{t-1}^c in the prototype re-balancing phase has drawbacks in the presence of high plasticity, as they may significantly differ from the real class means due to the training of the feature extractor (Eq. 12). Therefore, we propose a method to update the prototypes using the Empirical Feature Matrix, before performing the prototype re-balancing phase.

C. Prototype Drift Compensation via EFM

Fixed prototypes can become inaccurate over time due to drift from previous class representations. Yu et al. [24] showed that the drift in *embedding networks* can be estimated using current task data. They suggest estimating the drift of class means from previous-tasks by looking at feature drift in closely related classes from current task. They leveraged this drift to update class means in nearest-mean classification.

Let p_{t-1}^c the prototype of the class c at task $t-1$. Our aim is to update p_{t-1}^c after the training of task t to account for backbone drift. These updated prototypes are used for prototype rehearsal for training the model classifier. As proposed by SDC [24], we update the prototypes after the backbone is trained for each task as follows:

$$p_{t-1}^c \leftarrow p_{t-1}^c + \frac{\sum_{x_i \sim \mathcal{X}_t} w_i \delta_i}{\sum_{x_i \sim \mathcal{X}_t} w_i}, \quad \delta_i = f(x_i; \theta_t) - f(x_i, \theta_{t-1}), \quad (14)$$

where δ_i is the feature drift of samples x_i between task $t-1$ and t .

We define the weights w_i using the EFM (Figure 2b). In Section III-C we showed that the EFM induces a pseudo-metric in feature space, providing a second-order approximation of the KL-divergence due to feature drift. We extend the idea of feature drift estimation to softmax-based classifiers by weighting the overall drift of our class prototypes. Writing $p^c = p_{t-1}^c$ and $f_{t-1}(x_i) = f(x_i; \theta_{t-1})$ to simplify notation, our weights are defined as:

$$w_i = \exp\left(-\frac{(f_{t-1}(x_i) - p^c)E_{t-1}(f_{t-1}(x_i) - p^c)^\top}{2\sigma^2}\right) \approx \exp\left(-\frac{\text{KL}(p(y|f_{t-1}(x_i); W_{t-1}) || p(y|p^c; W_{t-1}))}{2\sigma^2}\right) \quad (15)$$

where E_{t-1} is the EFM after training task $t-1$. Eq. 15 assigns higher weights to the samples more closely aligned to prototypes in terms of probability distribution. Specifically, higher weights are assigned to samples whose softmax prediction matches that of the prototypes, indicating a strong similarity for the classifier.

Algorithm 1: Elastic Feature Consolidation with Prototype Re-balancing

```

Data:  $\mathcal{M}_1, E_1, \mathcal{P}_1$ 
for  $t = 2, \dots, T$  do
  /* Backbone Training */
  for each optimization step do
    sample  $\mathbf{X} \sim \mathcal{X}_t$ 
    compute  $\mathcal{L}_t^{\text{EFM}}$  (Eq. 10)
     $\mathcal{L}_t^{\text{train}} = \mathcal{L}_t^{\text{EFM}} + \mathcal{L}_t^{\text{ce}}(f(\mathbf{X}, \theta_t); W_{t-1:t})$  (Eq. 12)
    Update  $\theta_t \leftarrow \theta_t - \alpha_1 \frac{\partial \mathcal{L}_t^{\text{train}}}{\partial \theta_t}$ 
    Update  $W_{t-1:t} \leftarrow W_{t-1:t} - \alpha_2 \frac{\partial \mathcal{L}_t^{\text{train}}}{\partial W_{t-1:t}}$ 
  end
  /* Prototype Update */
   $\mathcal{P}_{1:t-1} \leftarrow \mathcal{P}_{1:t-1} + \Delta(E_{t-1})$  (Eqs. 14, 15)
  /* Prototype Re-balancing */
  for each optimization step do
    sample  $\mathbf{X} \sim \mathcal{X}_t, \tilde{\mathbf{P}} \sim \mathcal{P}_{1:t-1}$ 
     $\mathcal{L}_t^{\text{post-train}} = \mathcal{L}_t^{\text{ce}}(\tilde{\mathbf{P}} \cup f(\mathbf{X}, \theta_t^*); W_t)$  (Eq. 13)
    Update  $W_t \leftarrow W_t - \alpha_3 \frac{\partial \mathcal{L}_t^{\text{post-train}}}{\partial W_t}$ 
  end
   $\mathcal{P}_{1:t} \leftarrow \mathcal{P}_{1:t-1} \cup \mathcal{P}_t$ 
   $E_t \leftarrow \text{EFM}(\mathcal{X}_t, \mathcal{M}_t)$  (Eq. 8) /* Compute EFM */
end

```

D. Elastic Feature Consolidation++

To summarize, the training process begins with feature extractor training, where we optimize Eq. 12 to learn the new task while simultaneously regularize relevant directions from previous tasks (Figure 2a). Once the feature extractor is trained, we update the prototypes using the EFM (see Eqs. 14, 15 in Section IV-C), ensuring that representations from the previous task remain aligned with the current task drift (Figure 2b).

After updating the prototypes, we perform the *prototype re-balancing* phase to train the classifier (Eq. 13). Since the prototypes have already been aligned with the updated feature extractor, this guarantees that the classifier is trained with consistent representations (Figure 2c).

Finally, new prototypes and their corresponding class covariances are computed. The Empirical Feature Matrix E_t is then calculated using the current task data and to be used as regularizer for the next incremental task (Figure 2d).

We call this procedure, detailed in Algorithm 1, Elastic Feature Consolidation++ (EFC++) to highlight its extension of our previous approach, Elastic Feature Consolidation (EFC), introduced in [29]. In the next section, we demonstrate why EFC++ is more effective in Cold Start scenarios and how it differs from and improves upon EFC.

V. EFC++ MITIGATES THE PROTOTYPE-REHEARSAL SHORTCOMINGS OF EFC

In this section, we first briefly review Elastic Feature Consolidation (EFC) [29]. We then highlight the limitations of

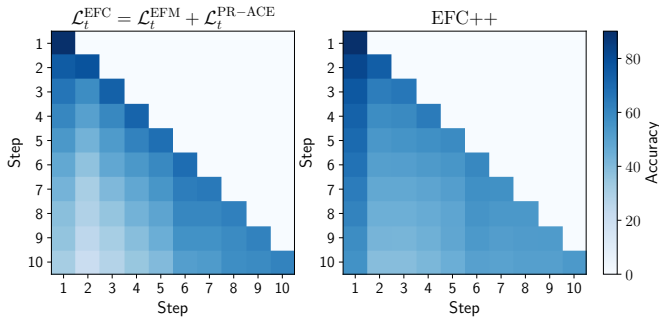


Fig. 4. Accuracy after each incremental step on the Cold Start CIFAR-100 10-step scenario. **Left:** In EFC, which combines EFM regularization with the asymmetric PR-ACE loss to balance current task data with prototypes during training, older tasks are forgotten more quickly than more recent ones. **Right:** EFC++, which applies EFM regularization during backbone training and a Prototype Re-balancing phase post-training, achieves a better plasticity-stability trade-off.

the prototype-rehearsal strategy employed by EFC and, finally, explain why and how EFC++, introduced in this extension, mitigates these issues.

A. Background: Elastic Feature Consolidation

Elastic Feature Consolidation (EFC) [29] is a combination of the empirical feature matrix loss $\mathcal{L}_t^{\text{EFM}}$ (Eq. 10), inhibiting drift in important directions for previous tasks, and an asymmetric cross-entropy loss (PR-ACE) balancing prototypes and new task samples during the current feature extractor training:

$$\mathcal{L}_t^{\text{EFC}} := \mathcal{L}_t^{\text{EFM}} + \mathcal{L}_t^{\text{PR-ACE}}, \quad (16)$$

where

$$\mathcal{L}_t^{\text{PR-ACE}} := \mathcal{L}_t^{\text{ce}}(f(\mathbf{X}, \theta_t); W_{t-1:t}) + \mathcal{L}_t^{\text{ce}}(\tilde{\mathbf{P}} \cup f(\hat{\mathbf{X}}, \theta_t); W_t). \quad (17)$$

Here $\mathbf{X}, \hat{\mathbf{X}} \sim \mathcal{X}_t$ are two distinct batches of current task data, while $\tilde{\mathbf{P}}$ is a batch of augmented prototypes, where each prototype $\tilde{p}_{t-1}^c \in \tilde{\mathbf{P}}$ is sampled from the Gaussian $\mathcal{N}(p_{t-1}^c, \Sigma^c)$. The term $\mathcal{L}_t^{\text{ce}}(f(\mathbf{X}, \theta_t); W_{t-1:t})$ is a cross-entropy loss restricted to the classes of the last task, while the term with prototypes $\mathcal{L}_t^{\text{ce}}(\tilde{\mathbf{P}} \cup f(\hat{\mathbf{X}}, \theta_t); W_t)$, affects old and current task classifier weights $W_t = [W_{t-1}, W_{t-1:t}]$.

Prototypes and current task features evaluated in the right term are uniformly sampled from all classes and used to train all task classifiers. Consequently, as the number of incremental steps increases, a larger proportion of prototypes is used compared to the current task data. After each task, the prototypes p_{t-1}^c are updated using Eq. 14 equipped with the EFM (Eq. 15) and new prototypes with the corresponding class covariances are computed. Finally, the EFM E_t is computed using the current task data to be used when learning subsequent incremental tasks (see Appendix C for the full training algorithm of EFC).

B. Limitations of PR-ACE in Cold Start

We identify limitations in using PR-ACE for training the final classifier. Since PR-ACE is applied during feature extractor training, the stored prototypes for previous classes gradually lose their representativeness of the true class means over the

course of current task epochs. This occurs because the feature space itself is evolving over time as a result of optimization, leading to a shift in the alignment between stored prototypes and their actual class means. Consequently, the classifier is trained with prototypes that increasingly deviate from the actual class means.

This misalignment is further compounded by the cross-entropy term $\mathcal{L}_t^{\text{ce}}(\tilde{\mathbf{P}} \cup f(\hat{\mathbf{X}}, \theta_t); W_t)$ on the right-hand side of Equation 17, which induces an *additional drift in the feature representation* along the relevant directions for previous tasks identified by the EFM. This drift arises from the backward pass on $\hat{\mathbf{X}}$, which updates the weights θ_t and alters the feature representations. Because PR-ACE uniformly samples prototypes $\tilde{\mathbf{P}}$ and new data $\hat{\mathbf{X}}$ based on class labels, mini-batches contain a larger proportion of current task data in earlier tasks compared to the later tasks. Consequently, earlier tasks undergo stronger representation drift (see Figure 5 for drift analysis).

For illustration, consider the Cold Start scenario where each task introduces an equal number of classes. In the second task, PR-ACE forms batches containing 50% prototypes and 50% image data; in the third task, this shift to two-thirds prototypes and one-third current data. Because the cross-entropy loss is averaged over both prototypes and new data, the gradient updates on the feature extractor become less severe for later tasks. As more tasks are added, the drift in the feature representation along the relevant directions of the EFM diminishes. Consequently, prototypes from earlier tasks remain farther from the actual class means than those from more recent tasks, leading to forgetting. This effect is illustrated in Figure 4 (left), where in EFC the performance on the first five tasks declines faster than on the last five.

Managing the drift caused by PR-ACE is particularly crucial in the Cold Start scenario, where, during initial training, a strong backbone cannot be learned, making the representations more susceptible to change compared to the Warm Start scenario (as we will show in Section VIII-B). In the next section, we describe how EFC++ effectively manages this drift and provide empirical evidence of its efficacy.

C. EFC++ addresses the PR-ACE limitations in Cold Start

EFC++ addresses the limitations of PR-ACE by decoupling the feature extractor training loss (Eq. 12) from inter-task classifier training via prototype-rehearsal (Eq. 13). This approach ensures that no additional drift occurs in the feature extractor while learning the current task, unlike in PR-ACE. Moreover, because EFC++ updates the prototypes before the post-training phase, the final classifier is trained using prototypes that more accurately reflect the real old class representations than those used by PR-ACE in EFC. As a result, *EFC++ more effectively controls drift in directions relevant to previous task classifiers without compromising plasticity* (see Figure 4, right).

To validate this claim, we consider a model continuously trained using either EFC or EFC++ up to task $t - 1$. We then measure the drift of the class means before and after training task t . Specifically, for each class $c \in \mathcal{C}_t$, we denote the feature representation of class c prior to task t by μ_{t-1}^c and after

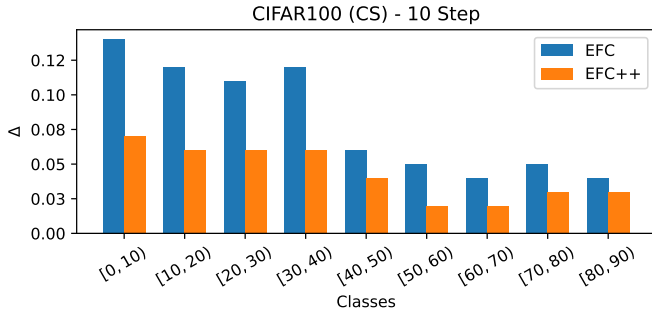


Fig. 5. Average drift of the class means in the relevant directions of the EFM before and after training the task in which they are involved, in both EFC and EFC++ on CIFAR-100 (CS) 10-step. EFC++ consistently exhibits less drift than EFC, especially in the initial tasks, where the drift of the classes is more pronounced (double) for EFC. This confirms that EFC++ better controls the drift along relevant directions.

training task t by μ_t^c . These representations are obtained by averaging the feature representations of the data for class c . We define the feature drift of the class mean as the difference between these feature representations, specifically,

$$\Delta\mu^c = \mu_t^c - \mu_{t-1}^c. \quad (18)$$

The squared pseudo-norm of $\Delta\mu^c$ via E_t , denoted as

$$\|\Delta\mu^c\|_{E_t} = (\Delta\mu)^T E_t \Delta\mu, \quad (19)$$

measures the magnitude of the drift of the class mean along the relevant directions identified after the training of task t . We then define the drift of task t as the average of the drifts of the class means, expressed as

$$\Delta = \frac{1}{|C_t|} \sum_{c \in C_t} \|\Delta\mu^c\|_{E_t}. \quad (20)$$

Figure 5 illustrates that, with EFC, the drift in the relevant directions due to PR-ACE is more pronounced in the earlier tasks compared to EFC++. In EFC++, decoupling the feature extractor training phase from the inter-task classifier learning phase allows for better control of the drift in the relevant directions. The reduction in drift along these directions does not compromise learning on the new classes. This is evidenced in Figure 4, which shows that the values on the diagonal of the confusion matrix for both EFC and EFC++ are comparable.

VI. EXPERIMENTAL SETTINGS

In this section, we describe the experimental setup used Elastic Feature Consolidation++ (EFC++) with the state-of-the-art in Exemplar-free Class-Incremental Learning (EFCIL).

A. Datasets

We evaluate EFC++ on five distinct datasets, with their statistics detailed in Appendix D-A. We categorize CIFAR-100 [65], Tiny-ImageNet [66], and ImageNet-Subset [67] as *small-scale* datasets, containing 100, 200, and 100 classes, respectively. For a more comprehensive *large-scale* scenario, we use ImageNet-1K [67], which includes 1000 diverse object classes with varying numbers of samples per class. Additionally, we utilize DN4IL, a well-crafted and balanced subset of the

TABLE I
CLASS DISTRIBUTION IN WARM START AND COLD START: $|C_0|$ IS THE NUMBER OF CLASSES IN THE PRE-TRAINING PHASE, WHILE $|C_{i>0}|$ REPRESENTS CLASSES INTRODUCED PER INCREMENTAL STEP.

Dataset	Warm Start (WS)		Cold Start (CS)	
	10 Step	20 Step	10 Step	20 Step
	$ C_0 $	$ C_{i>0} $	$ C_0 $	$ C_{i>0} $
CIFAR-100	50	5	40	3
Tiny-ImageNet	100	10	100	5
ImageNet-Subset	50	5	40	3
ImageNet-1K	500	50	400	30

standard DomainNet dataset [32]. DN4IL consists of 600 classes, with 100 classes per domain, specifically *clipart*, *infograph*, *painting*, *quickdraw*, *real*, and *sketch*. This dataset is instrumental in comparing our approach to the state-of-the-art under *large domain shifts*.

B. Warm and Cold Start Scenarios

We consider two scenarios for evaluating all approaches. The first, which we refer to as the **Warm Start (WS)** scenario which is commonly considered in the EFCIL literature [21], [22], [26], [23], involves pre-training the model on 50% or 40% of all available classes, denoted as C_0 . The remaining classes are then equally distributed among the subsequent incremental learning steps. This setting, which begins with a larger task favors continual learning techniques that prioritize *stability* in retained knowledge over the *plasticity* required to learn new classes.

The second scenario, which we call **Cold Start (CS)**, is relatively unexplored in the the recent EFCIL literature. In this scenario, the model is randomly initialized before incremental learning, and all available classes are equally split among the incremental learning steps, resulting in no initial pre-training phase. Consequently, the number of classes per step is larger compared to Warm Start. See Table I for a detailed description of how the classes are distributed in Warm Start and Cold Start across all datasets.

We are primarily interested in the Cold Start scenario since it demands high backbone plasticity and poses a significant challenge for EFCIL. Mitigating forgetting becomes difficult without using exemplars when larger backbone shifts occur (in Section VIII-B we provide an empirical analysis of this phenomenon).

C. Metrics

We use as metrics the **per-step incremental accuracy** A_{step}^K and **average incremental accuracy** A_{inc}^K :

$$A_{\text{step}}^K = \frac{\sum_{i=s}^K |C_i| a_i^K}{\sum_{i=s}^K |C_i|}, \quad A_{\text{inc}}^K = \frac{1}{K} \sum_{i=s}^K A_{\text{step}}^i, \quad (21)$$

where a_i^K represents the accuracy on task i after training task K , and $s = 1$ in the Cold Start scenario and $s = 0$ in the Warm Start scenario. It should be noted that in the Warm Start (WS) scenario, the performance on the initial classes, indicated as step $s = 0$, is commonly included in the evaluation metric [21], [23], [22], [26], [27], and we follow this same approach. Therefore,

achieving higher stability on the large number of initial classes significantly impacts the final evaluation. In contrast, in the Cold Start (CS) scenario the classes are equally distributed among the incremental learning tasks and the evaluation metrics starting from $s = 1$ give equal importance to each step.

To gain a more comprehensive understanding of impact of different regularization techniques employed by the tested methods, we use **average forgetting** F^K to measure stability during training and **cumulative average accuracy on the last task** PL^K to measure plasticity (i.e. the average of the diagonal of the matrix in Figure 4) [68]. More specifically, the forgetting of a task is the difference between its maximum accuracy obtained in the past and its current accuracy:

$$f_j^K = \max_{i \in \{s, \dots, k-1\}} (a_j^i - a_j^K), \quad j < K. \quad (22)$$

Thus, F^K and PL^K at the K -th task are defined as:

$$F^K = \frac{1}{K-1} \sum_{j=1}^{K-1} f_j^K, \quad PL^K = \frac{\sum_{i=s}^K |C_i| a_i^i}{\sum_{i=s}^K |C_i|}. \quad (23)$$

D. Hyperparameter settings

We use the standard ResNet-18 [1] trained from scratch for all experiments. We train the first task of each state-of-the-art method using the same optimizer, number of epochs, and data augmentations. In particular, we train the first task using self-rotation as in [21], [23] to align the performance of all techniques.

For the incremental steps of EFC++ we used Adam with a weight decay of $2e-4$ and a fixed learning rate of $1e-4$ for Tiny-ImageNet and CIFAR-100, while for ImageNet-Subset, ImageNet-1K, DN4IL we use a learning rate of $1e-5$ for the backbone and $1e-4$ for the heads. We fixed the total number of epochs to 100 and use a batch size of 64, except for ImageNet-1K where the batch size is fixed to 256. We set $\lambda_{EFM} = 10$ and $\eta = 0.1$ in Eq. 10 for all the experiments. In Section VIII-C, we discuss the theoretical basis for selecting these hyperparameters and analyze their impact on performance. For EFC++, during post-training we use SGD with a fixed learning rate $1e-3$ to train the final classifier on both prototype and current task features for 50 epochs.

We ran all approaches using five random seeds and shuffling the classes in order to reduce the bias induced by the choice of class ordering [40], [14]. In Appendix D-B we provide the optimization settings for each state-of-the-art method we evaluated.

VII. EXPERIMENTAL RESULTS

In this section we compare EFC++ with the state-of-the-art in Exemplar-free Class-Incremental Learning (EFCIL) on a variety of benchmarks. These include the small-scale Class-incremental (Class-IL) benchmarks (CIFAR-100, Tiny-ImageNet, and ImageNet-Subset), a large-scale Class-incremental benchmark (ImageNet-1K), and a large-scale Domain- and Class-incremental benchmark (DN4IL), using the last per-step A_{step}^K and average incremental accuracy A_{inc}^K . Most of the time, we reference the per-step accuracy when comparing performance, but similar conclusions can be drawn by considering the average incremental accuracy.

A. Small-scale Class-IL Experiments

In Table II we compare EFC++ with baselines and state-of-the-art EFCIL approaches. Specifically, we consider EWC [10], LwF [53], PASS [21], Fusion [23], FeTrIL [26], SSRE [22], FeCAM [27], ABD [31], R-DFCIL [30], and EFC [29] on both Warm and Cold Start scenarios for varying numbers of incremental steps. EFC++ significantly outperforms the previous state-of-the-art in both metrics across all scenarios and datasets.

Note that the incremental accuracy of SSRE and FeCAM in the Warm Start scenario differs from the values reported in the original paper, with SSRE higher and FeCAM lower. This discrepancy is attributable to the data augmentation policy we used and the self-rotation task we used initially to align all results with PASS and Fusion (both of which use self-rotation). This alignment is crucial when dealing with Warm Start scenarios, as performance on the large first task heavily biases the metrics (Eq. 21) as discussed in [69], [70]. In Appendix J-A and J-B we provide per-step performance plots in all the analyzed scenarios.

Warm Start. The experimental results on Warm Start scenarios (Table II, left) reveal that EFC++ exhibits substantial improvements (ranging from 2 to 6 percentage points), over recent methods like PASS, Fusion, FeTrIL, and SSRE across all benchmarks. In this setting, generative inversion-based methods (ABD, R-DFCIL) perform significantly worse than feature distillation approaches (PASS, Fusion, SSRE) and backbone freezing methods (FeTrIL, FeCAM). Compared to the newest and strongest competitor, FeCAM, EFC++ generally achieves better or comparable performance across all scenarios. Moreover, by comparing EFC++ and EFC, we see that the performance improvement is consistent regardless of the number of incremental learning steps. Specifically, for both CIFAR-100 and Tiny-ImageNet, in terms of per-step accuracy, EFC++ improves over EFC by approximately 1.3% and 1.7% for 10 and 20 steps, respectively; while for ImageNet-Subset EFC++ slightly improves the performance of EFC for both 10 and 20 incremental learning steps. This result is due that the drawback caused by the double backward pass required for computing $\mathcal{L}_t^{\text{PR-ACE}}$ in EFC, an effect reduced in the Warm Start scenario. This happens because the stronger backbone mitigates the overall drift, allowing EFC to perform almost as well as EFC++ in Warm Start (see Section VIII-B for drift comparison in WS and CS).

When comparing EFC++ with FeCAM, we observe that EFC++ achieves comparable performance on CIFAR-100, while on Tiny-ImageNet and ImageNet-Subset, it improves performance by approximately 1.2% in the 10-step scenario and remains comparable in the 20-step scenario. This is expected, as FeCAM, which freezes the backbone after the first task, is specifically designed for WS and benefits from

[†]Results of ABD and R-DFCIL on CIFAR-100 and Tiny-ImageNet are run using ResNet-18 for aligning all comparisons, while the original paper used ResNet-32 (except for ImageNet-Subset)

[‡]LwF results are not aligned with those in R-DFCIL, due to different architecture and implementation. We use the FACIL [14] implementation on ResNet-18, freezing old task classifier head while learning new task.

TABLE II

SMALL-SCALE CLASS-IL EXPERIMENTS. FUSION RESULTS ARE THOSE REPORTED IN [23] AS NO CODE IS PROVIDED TO REPRODUCE THEM. THE RESULT FOR IMAGENET-SUBSET COLD START FOR ABD AND R-DFCIL ARE THOSE REPORTED IN [30].

Method	Warm Start (WS)				Cold Start (CS)			
	A_{step}^K		A_{inc}^K		A_{step}^K		A_{inc}^K	
	10 Step	20 Step						
CIFAR-100								
EWC	21.08 ± 1.09	13.53 ± 1.11	41.00 ± 1.11	31.79 ± 2.77	31.17 ± 2.94	17.37 ± 2.43	49.14 ± 1.28	31.02 ± 1.15
LwF [‡]	20.73 ± 1.47	11.78 ± 0.60	41.95 ± 1.30	28.93 ± 1.62	32.80 ± 3.08	17.44 ± 0.73	53.91 ± 1.67	38.39 ± 1.05
PASS	53.42 ± 0.48	47.51 ± 0.37	63.42 ± 0.69	59.55 ± 0.97	30.45 ± 1.01	17.44 ± 0.69	47.86 ± 1.93	32.86 ± 1.03
Fusion	56.86	51.75	65.10	61.60	—	—	—	—
FeTrIL	56.79 ± 0.40	52.61 ± 0.81	65.03 ± 0.66	62.50 ± 1.03	34.94 ± 0.46	23.28 ± 1.24	51.20 ± 1.13	38.48 ± 1.07
SSRE	57.48 ± 0.55	52.98 ± 0.63	65.78 ± 0.59	63.11 ± 0.84	30.40 ± 0.74	17.52 ± 0.80	47.26 ± 1.91	32.45 ± 1.07
FeCAM	<u>62.13</u> ± 0.51	58.74 ± 0.60	<u>68.87</u> ± 0.40	67.42 ± 0.88	37.63 ± 0.52	23.82 ± 0.87	52.53 ± 1.19	38.51 ± 0.82
ABD [†]	44.91 ± 1.00	33.22 ± 1.11	56.81 ± 1.45	47.55 ± 0.19	43.11 ± 0.60	28.93 ± 0.21	<u>59.14</u> ± 1.72	47.12 ± 0.85
R-DFCIL [†]	52.24 ± 0.32	40.97 ± 0.12	63.09 ± 0.21	55.65 ± 0.10	42.14 ± 0.54	30.35 ± 0.05	57.77 ± 0.50	<u>47.41</u> ± 0.27
EFC	60.87 ± 0.39	55.78 ± 0.42	68.23 ± 0.68	65.90 ± 0.97	<u>43.62</u> ± 0.70	<u>32.15</u> ± 1.33	58.58 ± 0.91	47.36 ± 1.37
EFC++	62.15 ± 0.48	<u>57.55</u> ± 0.66	69.26 ± 0.63	<u>67.11</u> ± 0.91	47.52 ± 0.68	33.71 ± 1.41	61.57 ± 0.66	49.20 ± 1.10
Tiny-ImageNet								
EWC	6.73 ± 0.44	5.96 ± 1.17	18.48 ± 0.60	13.74 ± 0.52	8.00 ± 0.27	5.16 ± 0.54	24.01 ± 0.51	15.70 ± 0.35
LwF [‡]	24.00 ± 1.44	7.58 ± 0.37	43.15 ± 1.02	22.89 ± 0.64	26.09 ± 1.29	15.02 ± 0.67	45.14 ± 0.88	32.94 ± 0.54
PASS	41.67 ± 0.64	35.01 ± 0.39	51.18 ± 0.31	46.65 ± 0.47	24.11 ± 0.48	18.73 ± 1.43	39.25 ± 0.90	32.01 ± 1.68
Fusion	46.92	44.61	—	—	—	—	—	—
FeTrIL	45.71 ± 0.39	44.63 ± 0.49	53.95 ± 0.42	52.96 ± 0.45	30.97 ± 0.90	25.70 ± 0.61	45.60 ± 1.67	39.54 ± 1.19
SSRE	44.66 ± 0.45	44.68 ± 0.36	53.27 ± 0.43	52.94 ± 0.42	22.93 ± 0.95	17.34 ± 1.06	38.82 ± 1.99	30.62 ± 1.96
FeCAM	<u>50.77</u> ± 0.62	50.73 ± 0.46	<u>57.67</u> ± 0.48	<u>57.57</u> ± 0.37	30.79 ± 0.69	25.36 ± 0.74	45.00 ± 1.35	38.59 ± 1.29
ABD [†]	24.07 ± 1.08	11.17 ± 1.30	44.92 ± 1.41	34.70 ± 1.38	23.24 ± 0.57	12.21 ± 0.65	42.80 ± 1.07	33.37 ± 1.20
R-DFCIL [†]	43.06 ± 0.12	36.55 ± 0.06	53.39 ± 0.20	49.89 ± 0.25	<u>35.49</u> ± 0.25	28.23 ± 0.17	<u>49.14</u> ± 0.35	<u>42.30</u> ± 0.17
EFC	50.40 ± 0.25	48.68 ± 0.65	57.52 ± 0.43	56.52 ± 0.53	34.10 ± 0.77	<u>28.69</u> ± 0.40	47.95 ± 0.61	42.07 ± 0.96
EFC++	51.67 ± 0.31	<u>50.41</u> ± 0.51	58.54 ± 0.51	57.79 ± 0.54	37.48 ± 0.52	32.56 ± 0.44	50.18 ± 1.11	45.58 ± 1.32
ImageNet-Subset								
EWC	16.19 ± 2.48	10.66 ± 1.74	23.58 ± 2.01	18.05 ± 1.10	24.59 ± 4.13	12.78 ± 1.95	39.40 ± 3.05	26.95 ± 1.02
LwF [‡]	21.89 ± 0.52	13.24 ± 1.61	37.15 ± 2.47	25.96 ± 0.95	37.71 ± 2.53	18.64 ± 1.67	56.41 ± 1.03	40.23 ± 0.43
PASS	52.04 ± 1.06	44.03 ± 2.19	65.14 ± 0.36	58.88 ± 2.15	26.40 ± 1.33	14.38 ± 1.22	45.74 ± 0.18	31.65 ± 0.42
Fusion	60.20	51.60	70.00	63.70	—	—	—	—
FeTrIL	63.56 ± 0.59	57.62 ± 1.13	71.87 ± 1.46	68.01 ± 1.60	36.17 ± 1.18	26.63 ± 1.45	52.63 ± 0.56	42.43 ± 2.05
SSRE	61.84 ± 0.93	55.19 ± 0.97	70.68 ± 1.37	66.73 ± 1.61	25.42 ± 1.17	16.25 ± 1.05	43.76 ± 1.07	31.15 ± 1.53
FeCAM	67.68 ± 0.45	<u>62.74</u> ± 1.04	74.59 ± 0.94	<u>71.72</u> ± 1.45	35.54 ± 1.20	26.03 ± 1.33	51.90 ± 1.29	40.87 ± 2.00
ABD	38.68 ± 0.76	21.47 ± 2.08	55.72 ± 1.06	40.92 ± 2.30	35.96	22.40	57.76	44.89
R-DFCIL	49.81 ± 0.23	38.19 ± 0.13	64.50 ± 0.31	56.8 ± 0.69	42.28	30.28	59.10	47.33
EFC	<u>68.85</u> ± 0.58	62.17 ± 0.69	<u>75.40</u> ± 0.92	71.63 ± 1.13	<u>47.38</u> ± 1.43	<u>35.75</u> ± 1.74	<u>59.94</u> ± 1.38	<u>49.92</u> ± 2.05
EFC++	69.28 ± 0.46	62.75 ± 0.46	75.71 ± 1.00	72.05 ± 1.33	53.90 ± 1.18	40.86 ± 1.65	65.90 ± 1.62	55.42 ± 2.44

this constraint by preserving high first-task accuracy, which influences the final per-step accuracy. In contrast, our approach, which trains the feature extractor and enhances plasticity with the EFM regularizer, faces greater challenges in maintaining first-task performance, especially as the number of incremental steps increases. As a result, the per-step accuracy reflects this performance drop while remaining competitive with FeCAM (see Figure 6 for each task performance).

Cold Start. In Cold Start scenarios, (Table II, right), methods relying on feature distillation, such as SSRE and PASS, or those that freeze the feature extractor, such as FeTrIL and FeCAM, experience a significant decrease in accuracy compared to EFC++. This drop in accuracy is due the fact that the first task does not provide a sufficiently strong starting point for the entire class-incremental process. Moreover, most of these approaches exhibit weaker performance even when compared to LwF, which does not use prototypes to balance the classifiers.

Here, R-DFCIL, one of the *worst-performing* methods in the Warm Start scenario, achieves significantly better performance than all feature distillation approaches and methods that freeze the backbone. This highlights that the plasticity introduced by the knowledge distillation loss of R-DFCIL allows better learning of new tasks and as a result the final per-step accuracy assigning equal weights to all the tasks in this scenario is higher (see Eq. 21). Note that EFC++ outperforms R-DFCIL across all benchmarks. In terms of per-step accuracy, on CIFAR-100 it improves by 5% in the 10-step setting and by 3%

in the 20-step setting. On Tiny-ImageNet, it achieves a 2% improvement in 10-step and a 4% improvement in 20-step. Remarkably, on ImageNet-Subset it improves by 11% in 10-step and by 10% in 20-step. This increased gap is due to the generative mechanism used by R-DFCIL to rehearse old class samples, which becomes more challenging as image resolution increases (224 × 224 for ImageNet-Subset).

EFC++ *consistently and significantly improves the performance of EFC across all benchmarks and incremental learning steps.* The key reason is that, in the Cold Start scenario – where the backbone is trained with a small number of classes – feature drift is significant (see Section VIII-B for the drift comparison in WS and CS). In this setting, EFC++ better controls drift and achieves approximately 3-4 percentage points higher accuracy. Additionally, the improvement of EFC++ over EFC can be attributed to the decoupling of backbone training and the balancing of classification heads. This ensures that the prototypes used in EFC++ do not become outdated during training, unlike in EFC.

Per-task performance in WS and in CS. The results in the previous section clearly demonstrate that the challenges in Cold Start (CS) and Warm Start (WS) are different. Our results show that FeCAM performs well in WS, but struggles in CS due to reduced plasticity and poor feature representations for later tasks. Conversely, R-DFCIL excels in CS indicating strong plasticity, but underperforms in WS. EFC++ achieves comparable or better performance than FeCAM in WS and

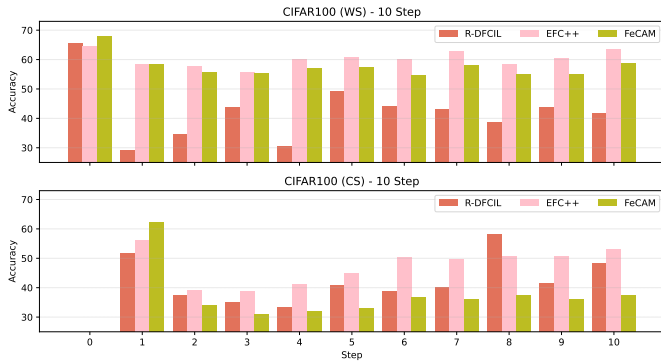


Fig. 6. Accuracy on each task after the final training step on CIFAR-100 Warm Start and Cold Start. EFC++ achieves the best stability-plasticity trade-off compared to the nearest competitor in Warm Start (FeCAM) and Cold Start (R-DFCIL).

TABLE III
LARGE SCALE CLASS- AND DOMAIN-IL EXPERIMENTS ON IMAGENET-1K (CS) AND DN4IL [32] (CS) USING A_{STEP}^K .

Method	ImageNet-1K (CS)		DN4IL (CS)
	10 Step	20 Step	6 Step
FeTrIL	34.28 ± 0.20	26.64 ± 0.25	30.95 ± 0.17
FeCAM	36.16 ± 0.10	27.24 ± 0.19	36.42 ± 0.12
R-DFCIL	29.36 ± 0.17	22.30 ± 0.19	22.31 ± 0.21
EFC	42.62 ± 0.08	36.32 ± 0.35	38.27 ± 0.16
EFC++	44.72 ± 0.11	37.46 ± 0.03	39.32 ± 0.15

outperforms all methods in CS, striking the best stability-plasticity trade-off.

Figure 6 shows task-wise accuracy after learning the final task on CIFAR-100 in both WS and CS. Task 0 represents the large first task in WS, which is absent in CS (see Table I). EFC++ achieves the best accuracy on new tasks, highlighting the effectiveness of the EFM regularizer in enhancing plasticity. While its first-task accuracy is lower than FeCAM in both settings, it remains competitive with R-DFCIL in WS and surpasses it in CS, reinforcing its overall stability-plasticity balance. It should be noted that R-DFCIL struggles on new tasks in WS, despite its strong plasticity in CS. We attribute this to the sampling strategy of R-DFCIL for retrieving old task data from the generative inversion-based model, which can struggle when the number of classes in subsequent tasks is significantly lower than in the first one, as in Warm Start.

B. Large-scale Domain- and Class-IL Experiments

In this section we evaluate EFC++ on large-scale incremental learning benchmarks.

Experiments on ImageNet-1K. We compare EFC++ with the nearest competitors in the Cold Start scenario on the large-scale ImageNet-1K dataset (see Table III) using final per-step accuracy. The average incremental accuracy for the Cold Start setting, as well as the per-step and average incremental accuracies for the Warm Start setting, can be found in Appendix F, where findings remain consistent with those on ImageNet-Subset.

Freezing the feature extractor limits the plasticity of FeTrIL and FeCAM, leading to accuracy drops of more than 6% and

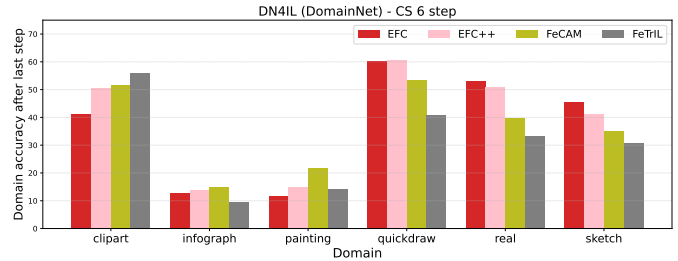


Fig. 7. Accuracy on each domain after the final training step on DN4IL. Methods that freeze the backbone, such as FeCAM and FeTrIL, achieve higher accuracy on the first domain, while EFC and EFC++ excel at learning new domains.

8%, respectively, compared to EFC and EFC++. Although R-DFCIL performs well in small-scale experiments, it now underperforms FeTrIL and FeCAM because its generative inversion network must learn to generate high-resolution images for 1,000 distinct classes by the end of the training (ten times more classes than Imagenet-Subset). Overall, EFC++ achieves the best performance, surpassing EFC by 2.1% in 10 steps and by 1.2% in 20 steps

Experiments on DN4IL (DomainNet). To further challenge our approach, we consider a domain- and class-incremental setting using the DN4IL dataset, a balanced subset of DomainNet. As shown in Table III, EFC++ improves upon EFC by approximately 1.1% in per-step accuracy and outperforms the remaining state-of-the-art approaches. EFC++ surpasses the best competitor, FeCAM, by roughly 3 points. R-DFCIL struggles here for reasons similar to those observed on ImageNet-1K. Additional comparisons are provided in Appendix F.

In Figure 7, we present per-task accuracy after the last training step (domain in this setting), showing that EFC++ achieves competitive performance on the first task compared to methods that freeze the backbone while maintaining better plasticity for learning new tasks. The only exception is the *painting* domain, where FeCAM performs better, and FeTrIL performs comparably. This is likely due to a stronger correlation between the first task and the third task. Comparing EFC++ with EFC, we observe that EFC++ achieves a better balance between plasticity and stability, since EFC loses nearly 10 points on the first task.

VIII. ABLATIONS AND ADDITIONAL ANALYSIS

In this section, we systematically ablate the key components of EFC++ to assess their individual contributions. We then analyze differences in feature representation drift between Warm Start and Cold Start scenarios, followed by a spectral analysis of the Empirical Feature Matrix and the impact of hyperparameter selection for EFM regularization. Finally, we discuss computational and storage requirements and examine the main limitations of EFC++, focusing on prototype rehearsal and covariance drift.

A. Ablation Studies

Ablation on EFM regularizer. We evaluate our proposed regularizer, EFM, against three established regularizer: Fisher

TABLE IV
ABLATION STUDY ON REGULARIZERS. WE REPORT THE FINAL AVERAGE FORGETTING (F^K), AVERAGE PLASTICITY (PL^K), AND PER-STEP ACCURACY (A_{STEP}^K) FOR CIFAR-100 AT 10 AND 20 STEPS.

Regularizer	CS - 10 Step			CS - 20 Step		
	$F^K(\downarrow)$	$PL^K(\uparrow)$	$A_{step}^K(\uparrow)$	$F^K(\downarrow)$	$PL^K(\uparrow)$	$A_{step}^K(\uparrow)$
E-FIM	67.28	84.27	23.72	71.98	83.22	14.83
KD	34.90	<u>70.67</u>	39.26	41.11	<u>65.41</u>	26.39
FD	12.67	51.83	<u>40.44</u>	8.78	35.85	<u>29.02</u>
EFM	<u>16.24</u>	62.72	47.52	<u>18.52</u>	50.79	33.71

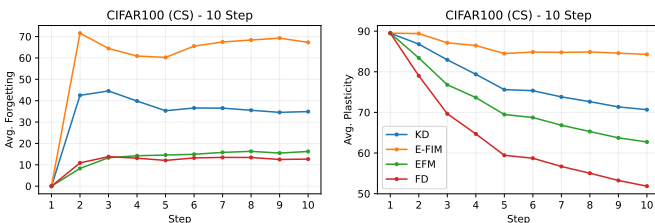


Fig. 8. Comparison of regularization methods on CIFAR-100 (CS) 10-step. EFM balances stability and plasticity, reducing forgetting (left) and improving plasticity (right) over FD. KD and EWC exhibit strong initial plasticity but suffer from severe forgetting after the first task.

Information Matrix (E-FIM, Eq. 3), Feature Distillation (FD, Eq. 5), and Knowledge Distillation (KD) [53]. To carry out this comparison, we directly replaced EFM regularization in our training framework without modifying any other components. Specifically, we maintained the same prototype updates and classifier rebalancing procedures. In order to perform these experiments, we carefully validate the hyperparameters associated with each regularizer (see Appendix H for more details on the validation). For these experiments, in addition to the per-step accuracy, we report the average forgetting and the average plasticity (see Eq. 23), to measure the stability and the plasticity induced by each regularizer. As shown in Table IV, EFM achieves the best trade-off between stability and plasticity, leading to the highest final accuracy in both the 10-step and 20-step settings on CIFAR-100. Figure 8 further highlights EFM effectiveness: its average forgetting (left) remains comparable to FD during the incremental steps, while its plasticity (right) is significantly improved. In contrast, while KD and E-FIM exhibit strong plasticity (right), they suffer from severe forgetting (left) after the first task, ultimately degrading their final performance as shown in Table IV.

Ablation on prototype update. In Table V we evaluate the effect of prototype updates using Eq. 14 and Eq. 15. Prototype updates significantly improve performance in both Warm Start and Cold Start across most benchmarks, except for ImageNet-Subset WS, where no significant improvement is observed.

B. Analysis of Feature Drift in Warm and Cold Start

We further investigate the role of high-quality feature representations in Warm Start and their relationship with feature drift during incremental learning. Our experimental results show that methodologies that freeze the backbone perform well in Warm Start but struggle in Cold Start. Moreover, the performance gains of EFC++ over EFC are more pronounced

TABLE V
ABLATION STUDY ON PROTOTYPE UPDATE. THE PERFORMANCE OF EFC++ IMPROVES WITH PROTOTYPE UPDATES IN BOTH WARM AND COLD START.

Dataset	Step	Update Proto (WS)		Update Proto (CS)	
		\times	\checkmark	\times	\checkmark
CIFAR-100	10	60.26 \pm 0.72	62.15 \pm 0.48	46.30 \pm 1.45	47.52 \pm 0.68
	20	56.10 \pm 0.34	57.55 \pm 0.66	31.71 \pm 2.26	33.71 \pm 1.41
Tiny-ImageNet	10	50.57 \pm 0.40	51.67 \pm 0.31	36.17 \pm 0.41	37.48 \pm 0.52
	20	46.86 \pm 1.19	50.41 \pm 0.51	29.04 \pm 0.65	32.56 \pm 0.44
ImageNet-Subset	10	69.09 \pm 0.30	69.28 \pm 0.46	52.95 \pm 1.00	53.90 \pm 1.18
	20	62.77 \pm 0.63	62.75 \pm 0.46	39.10 \pm 1.67	40.86 \pm 1.65

in Cold Start than in Warm Start, suggesting that the drift induced by PR-ACE has a smaller effect on final performance in Warm Start. This indicates that the initial quality of feature representations plays a crucial role on the final performance and on the drift occurring during incremental learning. In particular, *representations are less prone to change in Warm Start than in Cold Start, thanks to the strong initialization of the feature extractor.*

To empirically evaluate this, we propose applying EFC++ in two settings. In a Warm Start setting, the model is pre-trained on half of the available classes (i.e., $|C_0| = 50$ for CIFAR-100) and then incrementally trained for 10 steps, each with 5 classes per step ($|C_{i>0}| = 5$). In a Cold Start setting, the model starts with a random initialization (i.e., $|C_0| = 0$) and is then incrementally trained for 10 steps by following the same order and the same number of classes per step as in the Warm Start setting. Figure 9 presents the results of this analysis. For each set of classes (on the x -axis), we plot two lines representing the average distance between the actual class means (μ) and the estimated prototypes (p) throughout the experiment, with and without updates (dashed and solid lines, respectively) using the Empirical Feature Matrix as pseudo-metric. Comparing the two scenarios, we see that the average distance between the real class means and fixed prototypes is greater in the Cold Start setting, indicating that the representations are more prone to change compared to the Warm Start setting. Additionally, our prototype update rule (see Equations (14) and (15)) effectively mitigates prototype drift in both scenarios. However, it is less effective in the more challenging Cold Start scenario due to the greater representation drift.

C. EFM Spectral Analysis and Hyperparameters

Since EFC++ uses E_t to selectively regularize drift in feature space, it is natural to question *how* selective its regularization is. We can gain insight into this by analyzing how the rank of E_t evolves with increasing incremental tasks.

Consider training a model incrementally on CIFAR-100 using EFC++ up to the tenth and final task, computing along the way the spectrum of E_t for each $t \in [1, \dots, 10]$. We chose the ten task sequence for simplicity, but the same empirical conclusions hold regardless of the number of tasks. Recalling that $E_t \in \mathbb{R}^{n \times n}$ is symmetric, there then exist U_t and $\Lambda_t \in \mathbb{R}^{n \times n}$ such that $E_t = U_t^T \Lambda_t U_t$, where U_t is an orthogonal matrix and $\Lambda_t = \text{diag}(\lambda_1, \dots, \lambda_n)$ is a diagonal matrix whose entries contain the eigenvalues of E_t , sorted in descending

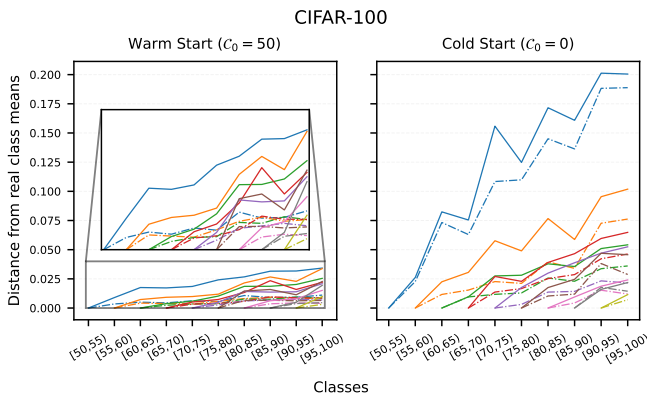


Fig. 9. Distance between real class means and prototypes when kept fixed (solid) or updated via the Empirical Feature Matrix (dashed) in both Warm and Cold Start scenarios on CIFAR-100 in EFC++. In Cold Start, the average distance of the prototypes from real class means change more than in Warm Start. Our prototype update rule effectively mitigates this drift.

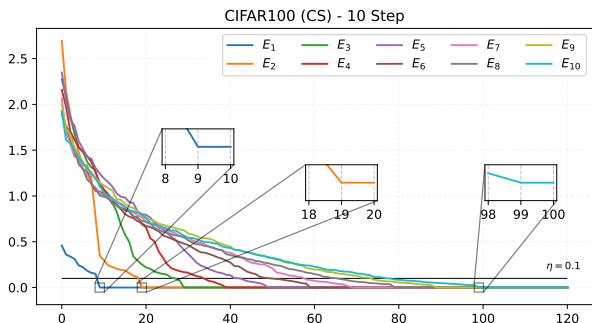


Fig. 10. The spectrum of the Empirical Feature Matrix across incremental learning steps. For a better visualization of the spectrum in the analysis we considered a Cold Start 10-step scenario on CIFAR-100. The x -axis is truncated at the 120th eigenvalue.

order. Since E_t is positive semi-definite, $\lambda_i \geq 0$ for each $i \in [1, \dots, n]$.

In Figure 10, we plot the spectrum of E_t at each $t \in [1, \dots, 10]$. This plot shows that the number of classes on which the matrix is estimated corresponds to an elbow in the curve beyond which the spectrum of the matrix vanishes. *This implies that the rank of the matrices is exactly equal to the number of observed classes minus one.*

Moreover, the horizontal line compares the magnitude of the eigenvalues across tasks with the damping term. Recalling that the results reported for EFC++ were obtained using parameter values of $\lambda_{\text{EFM}} = 10$ and $\eta = 0.1$, we observe that the plasticity constraints $\lambda_{\text{EFM}}\nu_i > \eta$ (described in Section III-C) are satisfied for nearly every $\nu_i > 0$, clearly demonstrating that *our regularizer effectively constrains the features in a non-isotropic manner, distinguishing it from feature distillation.*

To provide empirical proof of the importance of calibrating such hyperparameters (i.e., avoiding too low a value of η or degenerating into feature distillation), we also conducted a grid search testing 25 different combinations of λ_{EFM} and η . Figure 11 (left) shows that the selected combination achieves the peak value in terms of final per-step accuracy. In particular, it reveals that excessively low values of η lead to weaker regularization and increased forgetting (middle),

whereas excessively high values significantly reduce plasticity (right). See the Appendix G for a more comprehensive analysis on other scenarios.

D. Training Time and Memory Requirements

Training Time. FeTrIL and FeCaM are the fastest approaches as they freeze the backbone. Next is EWC, which does not apply any distillation and only E-FIM regularization. LwF, R-DFCIL, ABD, EFC, and EFC++ achieve comparable training times for the feature extractor, with two forward passes required for computing distillation losses in LwF, ABD and R-DFCIL, and two forward passes for computing EFM regularization in EFC and EFC++. SSRE slightly increases the training time due to architectural modifications introduced by the method. PASS is the most computationally expensive approach, as it applies self-rotation to each task, effectively doubling the training time.

In post-training, both EFC++, R-DFCIL and ABD introduce an additional computational overhead. However, the computation of EFM and prototypes in EFC++ is negligible compared to the training time, as it only requires a single forward pass over the backbone using the current task’s training dataset. Additionally, EFM can be computed without any backward pass (see Eq. 8). The prototype re-balancing phase takes approximately one-fifth of the time required for training the backbone, since the only classifier is trained and the feature extractor is frozen. In this phase, a single forward pass over the current training dataset is required to compute the task features because the feature extractor is frozen. The training time slightly increases across tasks due to the growing number of sampled prototypes.

R-DFCIL and ABD further extend training time by requiring the training of a deep generative inversion network after each task, which takes approximately 15 minutes – about three times longer than training the main model on CIFAR-100. This computation further increases when the resolution of the images to be generated increases (e.g. ImageNet).

Figure 12 shows the complete training times, with ABD and R-DFCIL omitted due to their significantly larger scale. Overall, when considering both its training and prototype re-balancing phases, EFC++ exhibits slightly higher training times compared to LwF and EFC, comparable timing to SSRE, and significantly lower training time than PASS. Training times were measured using an NVIDIA RTX 3090 GPU.

Memory requirements. EWC and LwF do not use prototypes, so no additional storage is required. FeTrIL, PASS, and SSRE need to store only class means. R-DFCIL increases storage requirements by including a generative deep inversion model with about 33M parameters (roughly 125.89 MB at 32-bit precision). EFC, EFC++, and FeCaM must store both class means and covariances. Comparing their memory requirements to R-DFCIL’s, storing 100 class covariance matrices of size 512x512 (as in CIFAR-100 with a ResNet-18 backbone) requires about 100 MB – slightly less than R-DFCIL. However, as the number of classes increases, the storage requirements for EFC, EFC++, and FeCaM grow with respect to R-DFCIL. In our previous work [29], we showed that these costs can be

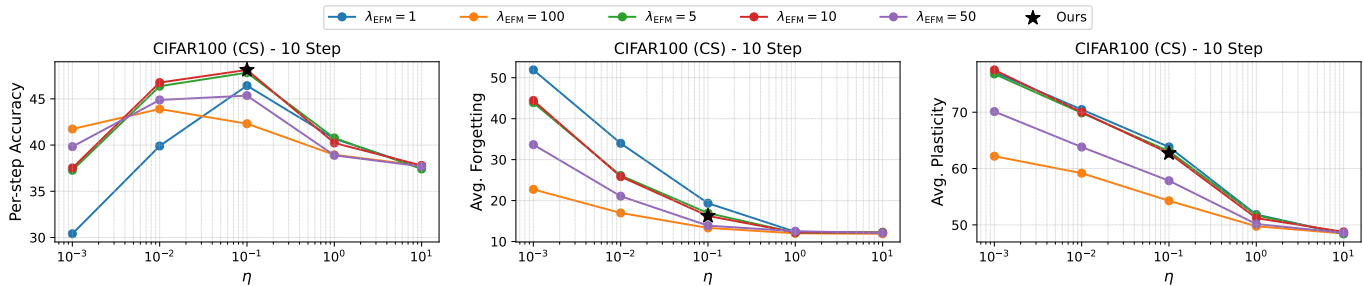


Fig. 11. A grid search testing 25 combinations of λ_{EFM} , with the x -axis in log scale for better visualization. **Left:** The selected combination, represented by the star symbol, achieves the peak per-step accuracy. **Middle:** Reducing the value of η weakens regularization and increases forgetting (see Eq. 23, left). **Right:** For high values of η , plasticity is significantly compromised (see Eq. 23, right).

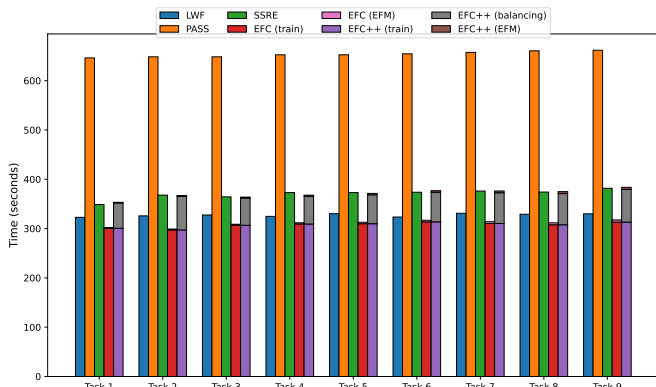


Fig. 12. Training times. For EFC++ we report the time required for backbone training, EFM and prototype computation, and the prototype re-balancing phase. Overall, EFC++ exhibits a slight increase in computational time compared to EFC and LwF, shows comparable timings to SSRE, and remains more efficient than PASS, R-DFCIL, and ABD. Timings for R-DFCIL and ABD are omitted as the deep inversion model training time alone already significantly exceeds the time required for the other approaches (about 15 minutes on CIFAR-100).

TABLE VI
IMPACT OF MEAN AND COVARIANCE DRIFT ON EFC++ (CIFAR-100 COLD START).

Step	Mean	Covariance	Accuracy	Delta
10	Fixed	Fixed	46.30 ± 1.45	—
	EFM	Fixed	47.52 ± 0.68	+1.22 (Ours)
	EFM	Real	47.37 ± 0.19	+1.07
	Real	Fixed	49.22 ± 0.17	+2.92
	Real	Real	49.33 ± 0.20	+3.03
20	Fixed	Fixed	31.71 ± 2.26	—
	EFM	Fixed	33.71 ± 1.41	+2.00 (Ours)
	EFM	Real	33.86 ± 1.49	+2.15
	Real	Fixed	37.04 ± 1.67	+5.33
	Real	Real	38.59 ± 1.64	+6.88
Joint Training			71.00	

mitigated through covariance approximation, thus eliminating the need to store a covariance matrix per class—or by applying a low-rank approximation. This significantly reduces storage without significant performance degradation.

E. Analysis of the limitations of EFC++

Since EFC++ does not update class covariances across incremental learning steps, we aim to understand how *covariance drift* affects the final performance. Table VI compares different update strategies of class statistics: our approach (class means estimated via EFM and fixed covariances, highlighted

in cyan) against an idealized setting using real mean and real covariances, computed from old task data fed in the current task backbone. While this strategy is infeasible in incremental learning – since past data is unavailable – it serves as an upper bound for performance and helps quantify the limitations of our prototype rehearsal strategy.

The results suggest that *updating the means via EFM and using real class covariances (third row) does not provide significant benefit*. However, replacing our estimated class means with real ones, while keeping the covariance fixed, leads to a substantial improvement: 2.92% and 5.33% with respect to having fixed statistics in 10 and 20 steps (fourth row). This confirms that challenges highlighted in Section VIII-B, that our approach encounters when estimating the real class drift in Cold Start. Using real class covariances significantly improves performance only as the number of steps increases (fifth row), but this improvement is much smaller compared to the impact of using real class means. In Appendix I we show that similar conclusion holds for Tiny-ImageNet and ImageNet-Subset.

From this analysis, we conclude that future work on Gaussian prototypes should prioritize more effective strategies for updating class means, beyond our current EFM approach. As a final note, we report the performance under Joint Training, where the gap remains substantial. Closing this gap will likely require either a more advanced strategy than Gaussian prototypes or improved regularization techniques beyond those we proposed.

IX. CONCLUSIONS

Exemplar-Free Class Incremental Learning requires a careful balance between model stability and plasticity. In this paper, we tackle the challenging Cold Start scenario in which inhibiting plasticity hinders the learning of novel tasks and caused a significant drop in incremental learning accuracy. We propose Elastic Feature Consolidation++ (EFC++), which consistently outperforms Elastic Feature Consolidation (EFC) across all benchmarks, further widening the gap with the state-of-the-art in Exemplar-Free Class Incremental Learning (EFCIL).

We derive an Empirical Feature Matrix (EFM) that induces a pseudo-metric used to control feature drift and improves plasticity with respect to the usage of feature distillation. We show that this matrix has interesting spectral properties depending on the number of classes in the incremental learning process. This matrix is also used to update prototypes, enabling

them to adapt to the feature space drift, which is particularly pronounced in the Cold Start scenario. These prototypes are leveraged in a prototype re-balancing phase to learn the inter-task classifier.

Overall, EFC++ achieves superior stability-plasticity trade-off compared to EFC across small-scale, large-scale, and domain-incremental learning benchmarks. This is achieved by applying the prototype re-balancing phase and a regularization on the feature space. Future works could develop and analyze more plastic regularizers, similar to EFM, applied to feature maps in the inner activations of the network. The interaction between increased plasticity across different layers is still unclear.

Driven in part by the development of foundation models, recent works have begun investigating incremental learning scenarios in which the initial backbone is pre-trained on massive datasets. In the future, we aim to investigate how strategies that enhance plasticity, like EFC++, perform in such pre-trained scenarios. We are particularly interested in understanding whether enhancing plasticity can improve performance when there is a large domain shift from the pre-training task, which is very common in real applications.

REFERENCES

- [1] K. He, X. Zhang, S. Ren, and J. Sun, "Deep residual learning for image recognition," *2016 IEEE Conference on Computer Vision and Pattern Recognition (CVPR)*, pp. 770–778, 2015.
- [2] A. Dosovitskiy, L. Beyer, A. Kolesnikov, D. Weissenborn, X. Zhai, T. Unterthiner, M. Dehghani, M. Minderer, G. Heigold, S. Gelly, J. Uszkoreit, and N. Houlsby, "An image is worth 16x16 words: Transformers for image recognition at scale," in *International Conference on Learning Representations*, 2021.
- [3] S. F. Ahmed, M. S. B. Alam, M. Hassan, M. R. Rozbu, T. Ishtiak, N. Rafa, M. Mofijur, A. B. M. Shawkat Ali, and A. H. Gandomi, "Deep learning modelling techniques: current progress, applications, advantages, and challenges," *Artificial Intelligence Review*, vol. 56, no. 11, pp. 13 521–13 617, Nov 2023.
- [4] K. Shaheen, M. A. Hanif, O. Hasan, and M. Shafique, "Continual learning for real-world autonomous systems: Algorithms, challenges and frameworks," *Journal of Intelligent & Robotic Systems*, vol. 105, no. 1, p. 9, Apr 2022.
- [5] S. Magistri, D. Baracchi, D. Shullani, A. D. Bagdanov, and A. Piva, "Continual learning for adaptive social network identification," *Pattern Recognition Letters*, vol. 180, pp. 82–89, 2024.
- [6] C. S. Lee and A. Y. Lee, "Clinical applications of continual learning machine learning," *The Lancet Digital Health*, vol. 2, no. 6, pp. e279–e281, Jun 2020.
- [7] W. Liu, X. Nie, B. Zhang, and X. Sun, "Incremental learning with open-set recognition for remote sensing image scene classification," *IEEE Transactions on Geoscience and Remote Sensing*, vol. 60, pp. 1–16, 2022.
- [8] M. McCloskey and N. J. Cohen, "Catastrophic interference in connectionist networks: The sequential learning problem," in *Psychology of learning and motivation*. Elsevier, 1989, vol. 24, pp. 109–165.
- [9] R. M. French, "Catastrophic forgetting in connectionist networks," *Trends in Cognitive Sciences*, vol. 3, no. 4, pp. 128–135, Apr 1999.
- [10] J. Kirkpatrick, R. Pascanu, N. Rabinowitz, J. Veness, G. Desjardins, A. A. Rusu, K. Milan, J. Quan, T. Ramalho, A. Grabska-Barwinska et al., "Overcoming catastrophic forgetting in neural networks," *Proceedings of the national academy of sciences*, vol. 114, no. 13, pp. 3521–3526, 2017.
- [11] E. Verwimp, R. Aljundi, S. Ben-David, M. Bethge, A. Cossu, A. Geppert, T. L. Hayes, E. Hüllermeier, C. Kanan, D. Kudithipudi, C. H. Lampert, M. Mundt, R. Pascanu, A. Popescu, A. S. Tolia, J. van de Weijer, B. Liu, V. Lomonaco, T. Tuytelaars, and G. M. van de Ven, "Continual learning: Applications and the road forward," *Transactions on Machine Learning Research*, 2024.
- [12] L. Wang, X. Zhang, H. Su, and J. Zhu, "A comprehensive survey of continual learning: Theory, method and application," *IEEE Transactions on Pattern Analysis and Machine Intelligence*, pp. 1–20, 2024.
- [13] M. Mermillod, A. Bugaiska, and P. BONIN, "The stability-plasticity dilemma: investigating the continuum from catastrophic forgetting to age-limited learning effects," *Frontiers in Psychology*, vol. 4, 2013.
- [14] M. Masana, X. Liu, B. Twardowski, M. Menta, A. D. Bagdanov, and J. Van De Weijer, "Class-incremental learning: survey and performance evaluation on image classification," *IEEE Transactions on Pattern Analysis and Machine Intelligence*, vol. 45, no. 5, pp. 5513–5533, 2022.
- [15] M. Kang, J. Park, and B. Han, "Class-incremental learning by knowledge distillation with adaptive feature consolidation," in *Proceedings of the IEEE/CVF conference on computer vision and pattern recognition*, 2022, pp. 16 071–16 080.
- [16] S. Yan, J. Xie, and X. He, "Der: Dynamically expandable representation for class incremental learning," in *Proceedings of the IEEE/CVF Conference on Computer Vision and Pattern Recognition*, 2021, pp. 3014–3023.
- [17] D.-W. Zhou, Q.-W. Wang, H.-J. Ye, and D.-C. Zhan, "A model or 603 exemplars: Towards memory-efficient class-incremental learning," in *The Eleventh International Conference on Learning Representations*, 2022.
- [18] X. Liu, M. Masana, L. Herranz, J. Van de Weijer, A. M. Lopez, and A. D. Bagdanov, "Rotate your networks: Better weight consolidation and less catastrophic forgetting," in *2018 24th International Conference on Pattern Recognition (ICPR)*. IEEE, 2018, pp. 2262–2268.
- [19] H. Ritter, A. Botev, and D. Barber, "Online structured laplace approximations for overcoming catastrophic forgetting," *Advances in Neural Information Processing Systems*, vol. 31, 2018.
- [20] X. Liu, C. Wu, M. Menta, L. Herranz, B. Raducanu, A. D. Bagdanov, S. Jui, and J. v. de Weijer, "Generative feature replay for class-incremental learning," in *Proceedings of the IEEE/CVF Conference on Computer Vision and Pattern Recognition Workshops*, 2020, pp. 226–227.
- [21] F. Zhu, X.-Y. Zhang, C. Wang, F. Yin, and C.-L. Liu, "Prototype augmentation and self-supervision for incremental learning," in *Proceedings of the IEEE/CVF Conference on Computer Vision and Pattern Recognition*, 2021, pp. 5871–5880.
- [22] K. Zhu, W. Zhai, Y. Cao, J. Luo, and Z.-J. Zha, "Self-sustaining representation expansion for non-exemplar class-incremental learning," in *Proceedings of the IEEE/CVF Conference on Computer Vision and Pattern Recognition*, 2022, pp. 9296–9305.
- [23] M. Toldo and M. Ozay, "Bring evanescent representations to life in lifelong class incremental learning," in *Proceedings of the IEEE/CVF Conference on Computer Vision and Pattern Recognition*, 2022, pp. 16 732–16 741.
- [24] L. Yu, B. Twardowski, X. Liu, L. Herranz, K. Wang, Y. Cheng, S. Jui, and J. v. d. Weijer, "Semantic drift compensation for class-incremental learning," in *Proceedings of the IEEE/CVF conference on computer vision and pattern recognition*, 2020, pp. 6982–6991.
- [25] A. Douillard, M. Cord, C. Ollion, T. Robert, and E. Valle, "Podnet: Pooled outputs distillation for small-tasks incremental learning," in *Computer Vision—ECCV 2020: 16th European Conference, Glasgow, UK, August 23–28, 2020, Proceedings, Part XX 16*. Springer, 2020, pp. 86–102.
- [26] G. Petit, A. Popescu, H. Schindler, D. Picard, and B. Delezoide, "Fetrl: Feature translation for exemplar-free class-incremental learning," in *Proceedings of the IEEE/CVF Winter Conference on Applications of Computer Vision*, 2023, pp. 3911–3920.
- [27] D. Goswami, Y. Liu, B. Twardowski, and J. van de Weijer, "FeCAM: Exploiting the heterogeneity of class distributions in exemplar-free continual learning," in *Thirty-seventh Conference on Neural Information Processing Systems*, 2023.
- [28] M. Davari, N. Asadi, S. Mudur, R. Aljundi, and E. Belilovsky, "Probing representation forgetting in supervised and unsupervised continual learning," in *Proceedings of the IEEE/CVF Conference on Computer Vision and Pattern Recognition (CVPR 2022)*, June 2022.
- [29] S. Magistri, T. Trinci, A. Soutif, J. van de Weijer, and A. D. Bagdanov, "Elastic feature consolidation for cold start exemplar-free incremental learning," in *The Twelfth International Conference on Learning Representations*, 2024.
- [30] Q. Gao, C. Zhao, B. Ghanem, and J. Zhang, "R-dfcil: Relation-guided representation learning for data-free class incremental learning," in *European Conference on Computer Vision*. Springer, 2022, pp. 423–439.
- [31] J. Smith, Y.-C. Hsu, J. Balloch, Y. Shen, H. Jin, and Z. Kira, "Always be dreaming: A new approach for data-free class-incremental learning," in *Proceedings of the IEEE/CVF International Conference on Computer Vision*, 2021, pp. 9374–9384.

- [32] S. Gowda, B. Zonooz, and E. Arani, “Dual cognitive architecture: Incorporating biases and multi-memory systems for lifelong learning,” *Transactions on Machine Learning Research*, 2023.
- [33] G. M. van de Ven, T. Tuytelaars, and A. S. Tolias, “Three types of incremental learning,” *Nature Machine Intelligence*, vol. 4, no. 12, pp. 1185–1197, Dec 2022.
- [34] M. De Lange, R. Aljundi, M. Masana, S. Parisot, X. Jia, A. Leonardis, G. Slabaugh, and T. Tuytelaars, “A continual learning survey: Defying forgetting in classification tasks,” *IEEE Transactions on Pattern Analysis and Machine Intelligence*, vol. 44, no. 7, pp. 3366–3385, 2022.
- [35] D. Lopez-Paz and M. A. Ranzato, “Gradient episodic memory for continual learning,” in *Advances in Neural Information Processing Systems*, I. Guyon, U. V. Luxburg, S. Bengio, H. Wallach, R. Fergus, S. Vishwanathan, and R. Garnett, Eds., vol. 30. Curran Associates, Inc., 2017.
- [36] R. Aljundi, E. Belilovsky, T. Tuytelaars, L. Charlin, M. Caccia, M. Lin, and L. Page-Caccia, “Online continual learning with maximal interfered retrieval,” in *Advances in Neural Information Processing Systems*, H. Wallach, H. Larochelle, A. Beygelzimer, F. d’Alché-Buc, E. Fox, and R. Garnett, Eds., vol. 32. Curran Associates, Inc., 2019.
- [37] Y. Zhang, B. Pfahringer, E. Frank, A. Bifet, N. J. S. Lim, and Y. Jia, “A simple but strong baseline for online continual learning: Repeated augmented rehearsal,” in *Advances in Neural Information Processing Systems*, vol. 35, 2022, pp. 14 771–14 783.
- [38] A. Soutif-Cormerais, A. Carta, A. Cossu, J. Hurtado, V. Lomonaco, J. Van de Weijer, and H. Hemati, “A comprehensive empirical evaluation on online continual learning,” in *Proceedings of the IEEE/CVF International Conference on Computer Vision*, 2023, pp. 3518–3528.
- [39] R. Aljundi, K. Kelchtermans, and T. Tuytelaars, “Task-free continual learning,” in *Proceedings of the IEEE/CVF Conference on Computer Vision and Pattern Recognition (CVPR)*, June 2019.
- [40] S.-A. Rebuffi, A. Kolesnikov, G. Sperl, and C. H. Lampert, “icarl: Incremental classifier and representation learning,” in *Proceedings of the IEEE conference on Computer Vision and Pattern Recognition*, 2017, pp. 2001–2010.
- [41] G. Hinton, O. Vinyals, and J. Dean, “Distilling the knowledge in a neural network,” *arXiv preprint arXiv:1503.02531*, 2015.
- [42] Y. Wu, Y. Chen, L. Wang, Y. Ye, Z. Liu, Y. Guo, and Y. Fu, “Large scale incremental learning,” in *Proceedings of the IEEE/CVF Conference on Computer Vision and Pattern Recognition (CVPR)*, June 2019.
- [43] E. Belouadah and A. Popescu, “Ii2m: Class incremental learning with dual memory,” in *Proceedings of the IEEE/CVF International Conference on Computer Vision (ICCV)*, October 2019.
- [44] P. Buzzega, M. Boschini, A. Porrello, D. Abati, and S. Calderara, “Dark experience for general continual learning: a strong, simple baseline,” *Advances in neural information processing systems*, vol. 33, pp. 15 920–15 930, 2020.
- [45] M. Boschini, L. Bonicelli, P. Buzzega, A. Porrello, and S. Calderara, “Class-incremental continual learning into the extended der-verse,” *IEEE Transactions on Pattern Analysis and Machine Intelligence*, vol. 45, no. 5, pp. 5497–5512, 2023.
- [46] S. Hou, X. Pan, C. C. Loy, Z. Wang, and D. Lin, “Learning a unified classifier incrementally via rebalancing,” in *Proceedings of the IEEE/CVF conference on computer vision and pattern recognition*, 2019, pp. 831–839.
- [47] Y. Liu, B. Schiele, and Q. Sun, “Adaptive aggregation networks for class-incremental learning,” in *Proceedings of the IEEE/CVF conference on Computer Vision and Pattern Recognition*, 2021, pp. 2544–2553.
- [48] F. Huszár, “Note on the quadratic penalties in elastic weight consolidation,” *Proceedings of the National Academy of Sciences*, vol. 115, no. 11, pp. E2496–E2497, 2018.
- [49] A. Chaudhry, P. K. Dokania, T. Ajanthan, and P. H. Torr, “Riemannian walk for incremental learning: Understanding forgetting and intransigence,” in *Proceedings of the European conference on computer vision (ECCV)*, 2018, pp. 532–547.
- [50] R. Aljundi, F. Babiloni, M. Elhoseiny, M. Rohrbach, and T. Tuytelaars, “Memory aware synapses: Learning what (not) to forget,” in *Proceedings of the European conference on computer vision (ECCV)*, 2018, pp. 139–154.
- [51] F. Zenke, B. Poole, and S. Ganguli, “Continual learning through synaptic intelligence,” in *Proceedings of the 34th International Conference on Machine Learning*, ser. Proceedings of Machine Learning Research, D. Precup and Y. W. Teh, Eds., vol. 70. PMLR, 06–11 Aug 2017, pp. 3987–3995.
- [52] F. Benzing, “Unifying importance based regularisation methods for continual learning,” in *Proceedings of The 25th International Conference on Artificial Intelligence and Statistics*, ser. Proceedings of Machine Learning Research, G. Camps-Valls, F. J. R. Ruiz, and I. Valera, Eds., vol. 151. PMLR, 28–30 Mar 2022, pp. 2372–2396.
- [53] Z. Li and D. Hoiem, “Learning without forgetting,” *IEEE transactions on pattern analysis and machine intelligence*, vol. 40, no. 12, pp. 2935–2947, 2017.
- [54] H. Jung, J. Ju, M. Jung, and J. Kim, “Less-forgetting learning in deep neural networks,” *arXiv preprint arXiv:1607.00122*, 2016.
- [55] F. Zhu, Z. Cheng, X.-y. Zhang, and C.-l. Liu, “Class-incremental learning via dual augmentation,” *Advances in Neural Information Processing Systems*, vol. 34, pp. 14 306–14 318, 2021.
- [56] E. Belouadah and A. Popescu, “Deesil: Deep-shallow incremental learning,” in *Proceedings of the European Conference on Computer Vision (ECCV) Workshops*, 2018.
- [57] H. Shin, J. K. Lee, J. Kim, and J. Kim, “Continual learning with deep generative replay,” in *Advances in Neural Information Processing Systems*, I. Guyon, U. V. Luxburg, S. Bengio, H. Wallach, R. Fergus, S. Vishwanathan, and R. Garnett, Eds., vol. 30. Curran Associates, Inc., 2017.
- [58] Y. Xiang, Y. Fu, P. Ji, and H. Huang, “Incremental learning using conditional adversarial networks,” in *Proceedings of the IEEE/CVF International Conference on Computer Vision (ICCV)*, October 2019.
- [59] A. Ayub and A. Wagner, “[{EEC}]: Learning to encode and regenerate images for continual learning,” in *International Conference on Learning Representations*, 2021.
- [60] C. Wang, J. Jiang, X. Hu, X. Liu, and X. Ji, “Enhancing consistency and mitigating bias: A data replay approach for incremental learning,” *Neural Networks*, vol. 184, p. 107053, 2025.
- [61] S.-I. Amari, “Natural gradient works efficiently in learning,” *Neural computation*, vol. 10, no. 2, pp. 251–276, 1998.
- [62] J. Martens, “New insights and perspectives on the natural gradient method,” *The Journal of Machine Learning Research*, vol. 21, no. 1, pp. 5776–5851, 2020.
- [63] L. Grentier and R. Fioresi, “Model-centric data manifold: the data through the eyes of the model,” *SIAM Journal on Imaging Sciences*, vol. 15, no. 3, pp. 1140–1156, 2022.
- [64] J. Martens and I. Sutskever, “Training deep and recurrent networks with hessian-free optimization,” in *Neural Networks: Tricks of the Trade: Second Edition*. Springer, 2012, pp. 479–535.
- [65] A. Krizhevsky, G. Hinton *et al.*, “Learning multiple layers of features from tiny images,” *Technical report*, 2009.
- [66] J. Wu, Q. Zhang, and G. Xu, “Tiny imagenet challenge,” *Technical report*, 2017.
- [67] J. Deng, W. Dong, R. Socher, L.-J. Li, K. Li, and L. Fei-Fei, “Imagenet: A large-scale hierarchical image database,” in *2009 IEEE conference on computer vision and pattern recognition*. Ieee, 2009, pp. 248–255.
- [68] M. D. Lange, G. M. van de Ven, and T. Tuytelaars, “Continual evaluation for lifelong learning: Identifying the stability gap,” in *The Eleventh International Conference on Learning Representations*, 2023.
- [69] D.-W. Zhou, Q.-W. Wang, Z.-H. Qi, H.-J. Ye, D.-C. Zhan, and Z. Liu, “Deep class-incremental learning: A survey,” *arXiv preprint arXiv:2302.03648*, 2023.
- [70] F. M. Castro, M. J. Marín-Jiménez, N. Guil, C. Schmid, and K. Alahari, “End-to-end incremental learning,” in *Proceedings of the European conference on computer vision (ECCV)*, 2018, pp. 233–248.
- [71] D. P. Kingma and J. Ba, “Adam: A method for stochastic optimization,” *arXiv preprint arXiv:1412.6980*, 2014.

Simone Magistri earned his PhD in Smart Computing from Florence University, Italy, in 2024. He is currently a Postdoctoral Researcher at the Information Engineering Department in Florence, Italy. His research interests encompass deep learning, computer vision, continual learning techniques, and their applications.

Tommaso Trinci gained his master’s degree in Mathematics at the University of Florence, Italy, in 2018. He is currently PhD student in Information Engineering at the University of Florence. His research interests include deep learning, computer vision and green AI.

Albin-Soutif Cormerais earned his PhD in Computer Science, from the autonomous university of Barcelona, Spain, in 2024. His research interests revolve around deep learning, continual learning and online learning.

Joost van de Weijer received the PhD degree from the University of Amsterdam, in 2005. He was a Marie Curie Intra-European fellow with INRIA Rhone-Alpes, France, and from 2008 to 2012 was a Ramon y Cajal fellow with the Universitat Autònoma de Barcelona, Spain, where he is currently a senior scientist with the Computer Vision Center and leader of the LAMP Team.

Andrew D. Bagdanov received the PhD degree from the University of Amsterdam, in 2004, after which he was a postdoc with the University of Florence and the Universitat Autònoma de Barcelona, and was a Ramon y Cajal fellow with the Computer Vision Center, Barcelona. He is associate professor with the University of Florence, Italy. His research spans a broad spectrum of computer vision, image processing and machine learning.

APPENDIX

APPENDIX A

SCOPE AND SUMMARY NOTATION

In these appendices, we provide the analytical formulation of the Empirical Feature Matrix (Section B), the algorithm for Elastic Feature Consolidation (Section C), dataset and optimization details (Section D), additional insights on the experiments (Section E and Section F), extensive validation of our regularization hyperparameters (Section G), further ablation studies (Section H), an analysis on the limitations of prototype rehearsal in EFC++ (Section I) and finally, per-step plots for Warm Start and Cold Start scenarios for the small-scale class-IL experiments (Section J).

For convenience, we summarize here the notation used in the paper:

- \mathcal{M}_t : the incremental model at task t .
- K : the total number of tasks.
- \mathcal{C}_t : the set of classes associated with task t .
- \mathcal{D} : the incremental dataset containing samples \mathcal{X}_t and labels \mathcal{Y}_t for each task t .
- $f(\cdot; \theta_t)$: The feature vector computed by the backbone at task t with parameters θ_t .
- n : the dimensionality of the feature space.
- W_t : the classifier at task t with dimensions $\mathbb{R}^{n \times \sum_{j=1}^t |c_j|}$.
- E_t : empirical feature matrix computed at task t .
- λ_{EFM} : hyperparameter associated to the Empirical Feature Matrix, Eq. 10 in the main paper.
- η : damping hyperparameter associated to the Identity Matrix, Eq. 10 in the main paper.
- $\mathbf{X} \sim \mathcal{X}_t$: a batch of current task data.
- $\mathcal{P}_{1:t-1}$: prototypes accumulated up to the task $t-1$.
- $\tilde{\mathbf{P}} \sim \mathcal{P}_{1:t-1}$: a batch of prototypes with Gaussian perturbation.
- A_{step}^K and A_{inc}^K : the per-step incremental accuracy and the average incremental accuracy, Eq. 21 in the main paper.
- F^K and PL^K : the average forgetting and the cumulative average accuracy on the last task, Eq. 23 in the main paper.

APPENDIX B

THE EMPIRICAL FEATURE MATRIX

In this appendix we derive an analytic formulation of the local features matrix defined in the main paper in Section III-C. To simplify the notation, we recall its definition without explicitly specifying the task, as it is unnecessary for the derivation:

$$E_{f(x)} = \mathbb{E}_{y \sim p(y)} \left[\left(\frac{\partial \log p(y)}{\partial f(x)} \right) \left(\frac{\partial \log p(y)}{\partial f(x)} \right)^\top \right]. \quad (24)$$

We begin by computing the Jacobian matrix with respect to the feature space of the output function $g: \mathbb{R}^m \rightarrow \mathbb{R}^m$ which is the log-likelihood of the model on logits z :

$$g(z) = \log(\text{softmax}(z)) = [\log(\sigma_1(z)), \dots, \log(\sigma_m(z))]^\top,$$

where

$$\sigma_i(z) = \frac{e^{z_i}}{\sum_{j=1}^m e^{z_j}}.$$

The partial derivatives of g with respect to each input z_i are:

$$\frac{\partial \log(\sigma_i(z))}{\partial z_j} = \begin{cases} 1 - \sigma_i(z) & \text{if } i = j, \\ -\sigma_j(z) & \text{otherwise.} \end{cases} \quad (25)$$

Thus, the Jacobian matrix of g is:

$$J(z) = \begin{bmatrix} 1 - \sigma_1(z) & -\sigma_2(z) & \dots & -\sigma_m(z) \\ -\sigma_1(z) & 1 - \sigma_2(z) & & \vdots \\ \vdots & & \ddots & \\ -\sigma_1(z) & \dots & & 1 - \sigma_m(z) \end{bmatrix} \quad (26)$$

$$= I_m - \mathbb{1}_m \cdot \begin{bmatrix} \sigma_1(z) \\ \vdots \\ \sigma_m(z) \end{bmatrix}^\top = I_m - P, \quad (27)$$

where $I_m \in \mathbb{R}^{m \times m}$ is the identity matrix and $\mathbb{1}_m$ represent the vector with all entries equal to 1.

Recalling Eq. 24, we are interested in computing the derivatives of the log-probability vector with respect to the feature vector:

$$\frac{\partial \log p(y_1, \dots, y_m | f; W)}{\partial f} = \frac{\partial(Wf)}{\partial f} \frac{\partial(\log(\sigma(z)))}{\partial z} \quad (28)$$

$$= WJ(z), \quad (29)$$

where $z = Wf$ for W the classifier weight matrix mapping features f to logits z . Combining this with Eq. 27 we have:

$$E_{f(x)} = \mathbb{E}_{y \sim p(y)} \left[W(I_m - P)_y (W(I_m - P)_y)^\top \right], \quad (30)$$

where $p(y) = p(y|f(x); W)$, P is the matrix containing the probability vector associated with f in each row, and $(I_m - P)_y$ is the column vector containing the y_{th} row of the Jacobian matrix. Computing E_t using Eq. 30 requires only a single forward pass of all data through the network, whereas a naive implementation requires an additional backward pass up to the feature embedding layer.

APPENDIX C

ELASTIC FEATURE CONSOLIDATION ALGORITHM

For completeness we show in Algorithm 2 the pseudocode for Elastic Feature Consolidation, which uses the asymmetric cross-entropy loss instead of the prototype rebalancing phase as in EFC++. All the equations refer to the main paper.

APPENDIX D

DATASET, IMPLEMENTATION AND HYPERPARAMETER SETTINGS

In this section we expand the discussion of Section VI-A and Section VI-D of the main paper by providing additional information about the dataset and the implementation of the approaches we tested.

Algorithm 2: Elastic Feature Consolidation

```

Data:  $\mathcal{M}_1, E_1, \mathcal{P}_1$ 
for  $t = 2, \dots, T$  do
  /* Backbone and Classifier Train */
  for each optimization step do
    sample  $\mathbf{X} \sim \mathcal{X}_t, \tilde{\mathbf{P}} \sim \mathcal{P}_{1:t-1}$ 
    compute  $\mathcal{L}_t^{\text{EFM}}$  (Eq. 10)
    compute  $\mathcal{L}_t^{\text{PR-ACE}}$  (Eq. 17)
     $\mathcal{L}_t^{\text{EFC}} \leftarrow \mathcal{L}_t^{\text{PR-ACE}} + \mathcal{L}_t^{\text{EFM}}$ 
    Update  $\theta_t \leftarrow \theta_t - \alpha \frac{\partial \mathcal{L}_t^{\text{EFC}}}{\partial \theta_t}$ 
    Update  $W_t \leftarrow W_t - \alpha \frac{\partial \mathcal{L}_t^{\text{EFC}}}{\partial W_t}$ 
  end

  /* Prototype Update */
   $\mathcal{P}_{1:t-1} \leftarrow \mathcal{P}_{1:t-1} + \Delta(E_{t-1})$  (Eqs. 14, 15)
   $\mathcal{P}_{1:t} \leftarrow \mathcal{P}_{1:t-1} \cup \mathcal{P}_t$ 

  /* EFM Calculus */
   $E_t \leftarrow \text{EFM}(\mathcal{X}_t, \mathcal{M}_t)$  (Eq. 8)
end

```

A. Datasets

We perform our experimental evaluation on four standard datasets. CIFAR-100 [65] consists of 60,000 images divided into 100 classes, with 600 images per class (500 for training and 100 for testing). ImageNet-1K is the original ImageNet dataset [67], consisting of about 1.3 million images divided into 1,000 classes. Tiny-ImageNet [66] consists of 100,000 images divided into 200 classes, which are taken from ImageNet and resized to 64×64 pixels. ImageNet-Subset is a subset of the original ImageNet dataset that consists of 100 classes. The images are resized to 224×224 pixels. DNIL [32] is a balance subset of DomainNet and it consists of six domains, each with 100 classes, and a total of 85,000 images. The images are resized to 224×224 pixels. Each domain (i.e. *clipart*, *infograph*, *painting*, *quickdraw*, *real*, and *sketch*) is treated as a different task, resulting in a 6-step scenario used to evaluate the performance when large domain shifts occur.

B. Implementation and Hyperparameters

For all the methods, we use the standard ResNet-18 [1] backbone trained from scratch.

First Task Optimization Details. We use the same optimization settings for both the Warm Start and Cold Start scenarios. We train the models on CIFAR-100 and on Tiny-ImageNet for 100 epochs with Adam [71] using an initial learning rate of $1e^{-3}$ and fixed weight decay of $2e^{-4}$. The learning rate is reduced by a factor of 0.1 after 45 and 90 epochs (as done in [21], [23]). For ImageNet-Subset, we followed the implementation of PASS [21], fixing the number of epochs at 160, and used Stochastic Gradient Descent with an initial learning rate of 0.1, momentum of 0.9, and weight decay of $5e^{-4}$. The learning rate was reduced by a factor of 0.1 after 80, 120, and 150 epochs. We applied the same label and data augmentation (random crops and flips) for all the evaluated datasets. For the first task

of each dataset, we use self-rotation as performed by [21], [23]. For both ImageNet-1k and DN4IL, we apply the same hyperparameters and training protocol used for the ImageNet-Subset. The batch size is set to 64 for DN4IL and 256 for ImageNet-1k. For ImageNet-1k, self-rotation is deactivated for the first task.

Incremental Steps. Below we provide the hyperparameters and the optimization settings we used for the incremental steps of each state-of-the-art method we tested.

- **EWC [10]:** We used the implementation of [14]. Specifically, we configured the coefficient associated to the regularizer as $\lambda_{\text{E-FIM}} = 5000$ and the fusion of the old and new importance weights is done with $\alpha = 0.5$. For the incremental steps we fix the total number of epochs to 100 and we use Adam optimizer with an initial learning rate of $1e^{-3}$ and fixed weight decay of $2e^{-4}$. The learning rate is reduced by a factor of 0.1 after 45 and 90 epochs.
- **LwF [53]:** We used the implementation of [14]. In particular, we set the temperature parameter $T = 2$ as proposed in the original work and the parameter associated to the regularizer λ_{LwF} to 10. For the incremental steps we fix the total number of epochs to 100 and we use Adam optimizer with an initial learning rate of $1e^{-3}$ and fixed weight decay of $2e^{-4}$. The learning rate is reduced by a factor of 0.1 after 45 and 90 epochs.
- **PASS [21]:** We follow the implementation provided by the authors. It is an approach relying upon feature distillation and prototypes generation. Following the original paper we set $\lambda_{\text{FD}} = 10$ and $\lambda_{\text{pr}} = 10$. In the original code, we find a temperature parameter, denoted as T , applied to the classification loss, which we set to $T = 1$. As provided in the original paper, for the incremental steps we fix the total number of epochs to 100 and we use Adam optimizer with an initial learning rate of $1e^{-3}$ and fixed weight decay of $2e^{-4}$. The learning rate is reduced by a factor of 0.1 after 45 and 90 epochs
- **SSRE [22]:** We follow the implementation provided by the authors. It is an approach relying upon feature distillation and prototypes generation. Following the original paper, we set $\lambda_{\text{FD}} = 10$ and $\lambda_{\text{pr}} = 10$. In the original code, we find a temperature parameter, denoted as T , applied to the classification loss, which we set to $T = 1$. Following the code, for the incremental steps we fixed the total number of epochs to 60 and used Adam with an initial learning rate of $2e^{-4}$ and fixed weight decay of $5e^{-4}$. The learning rate is reduced by a factor of 0.1 after 45 epochs.
- **FeTrIL [26]:** We follow the official code provided by the authors. During the incremental steps, it uses a Linear SVM classifier working on the pseudo-features extracted from the frozen backbone after the first task. We set the SVM regularization $C = 1$ and the tolerance to 0.0001 as provided by the authors.
- **FeCAM [27]:** We follow the implementation provided by the authors. During the steps, it uses Mahalanobis-based distance for classification on the features extracted from the frozen backbone after the first task and transformed via Tukey’s Ladder of Powers transformation. To improve and

stabilize the Mahalanobis-based distance classification, it applies covariance normalization and covariance shrinkage. Following the original implementation, we set the hyperparameter of Tukey’s Ladder of Powers transformation, λ , to 0.5 and the hyperparameters of the covariance shrinkage, γ_1 and γ_2 , to 1.

- **Deep Inversion Methods:** We trained ABD [31] and R-DFCIL [30] following their official implementations. The only difference from the original papers is that CIFAR-100 and Tiny-ImageNet were tested using a ResNet-32 [1] backbone. However, for a fair comparison, we replaced it with ResNet-18. Regarding optimization details, we follow the same settings originally used by the authors for ImageNet-Subset, where they employed ResNet-18. Specifically, we train all benchmarks for 100 epochs for ABD and 120 epochs for R-DFCIL, using SGD with an initial learning rate of 0.1 for CIFAR-100, Tiny-ImageNet, and DN4IL, and 0.005 for ImageNet-Subset and ImageNet-1K, following the original learning rate schedule*. We apply a fixed weight decay of $1e^{-4}$ and a momentum of 0.9. The batch size is set to 128 for CIFAR-100 and Tiny-ImageNet, while for DN4IL, ImageNet-Subset, and ImageNet-1K, it is 64. We use the same deep inversion network, running 10,000 inversion iterations for CIFAR-100 and Tiny-ImageNet, and 50,000 iterations for ImageNet-Subset and ImageNet-1K.

APPENDIX E

SMALL-SCALE CLASS-IL EXPERIMENTS

In Figure 6 of the main paper, we present the accuracy on each CIFAR-100 task after the final training step for both the Warm and Cold start scenarios. In Figure 13, we provide a similar plot for the remaining small-scale benchmarks. The results again confirm that the approaches exhibit significantly different performance in the Warm start versus Cold start settings, reflecting their respective stability-plasticity trade-offs.

APPENDIX F

LARGE-SCALE CLASS- AND DOMAIN-INCREMENTAL LEARNING

In this section, we evaluate EFC++ on large-scale incremental learning benchmarks, integrating the results from Section VII-B of the main paper.

Experiments on ImageNet-1K Table VII completes the results presented in Table III of the main paper for ImageNet-1K. As already discussed in Section VII-B, EFC++ achieves remarkable results in the Cold Start scenario compared to all other competitors, while in the Warm Start setting, it achieves performance comparable to FeCAM and EFC. This can be explained by observing that the generalization gained on the large first task in a large-scale dataset reduces the necessity for plasticity when learning new tasks, thereby aligning the performance across these approaches. It must be noted that the results reported in [26] are slightly better in the Warm Start

*We chose not to test ABD on DN4IL and ImageNet-1K because it generally performs worse than R-DFCIL on all other datasets.

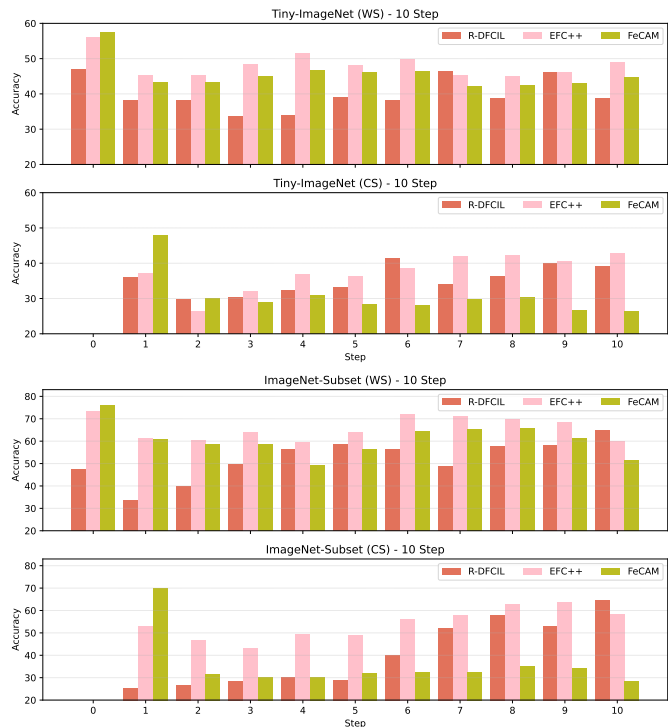


Fig. 13. Accuracy on each task after the final training step on Tiny-ImageNet and ImageNet-Subset Warm Start and Cold Start. EFC++ achieves the best stability-plasticity trade-off compared to the nearest competitor in Warm Start (FeCAM) and Cold Start (R-DFCIL).

TABLE VII

LARGE SCALE CLASS-INCREMENTAL EXPERIMENTS. WE COMPARE WITH THE STATE-OF-THE-ART ON IMAGENET-1K.

	Method	A_{step}^K		A_{inc}^K	
		10 Step	20 Step	10 Step	20 Step
WS	FeTrIL	55.26 ± 0.16	51.10 ± 0.22	63.42 ± 0.08	60.93 ± 0.12
	FeCAM	58.73 ± 0.09	55.67 ± 0.16	65.83 ± 0.14	64.22 ± 0.14
	R-DFCIL	35.47 ± 0.19	29.27 ± 0.53	46.42 ± 0.18	42.13 ± 0.58
	EFC	59.49 ± 0.07	55.94 ± 0.09	66.64 ± 0.10	64.89 ± 0.10
	EFC++	<u>59.09 ± 0.15</u>	54.82 ± 0.17	<u>66.43 ± 0.11</u>	<u>64.45 ± 0.20</u>
CS	FeTrIL	34.28 ± 0.20	26.64 ± 0.25	48.93 ± 0.15	40.02 ± 0.15
	FeCAM	36.16 ± 0.10	27.24 ± 0.19	50.38 ± 0.14	40.67 ± 0.24
	R-DFCIL	29.36 ± 0.17	22.30 ± 0.19	40.86 ± 0.37	34.95 ± 0.17
	EFC	<u>42.62 ± 0.08</u>	<u>36.32 ± 0.35</u>	<u>56.52 ± 0.10</u>	<u>49.80 ± 0.20</u>
	EFC++	44.72 ± 0.11	37.46 ± 0.03	58.39 ± 0.16	52.34 ± 0.11

scenario in terms of average incremental accuracy compared to those reported in Table VII. This gap is likely due to the performance on the initial task, which has a significant impact on average incremental accuracy. Finally, as already observed in Section VII-B, R-DFCIL struggles in large-scale scenarios regardless of the number of classes in the first task. This is because its generative inversion network must learn to generate high-resolution images for 1,000 distinct classes.

Experiments on DN4IL (DomainNet). Table VIII extends Table 3 of the main paper for DN4IL by adding results for EwC, LwF, PASS, and SSRE, while also reporting the average incremental accuracy for all approaches. Among all the approaches, only FeCAM and SSRE achieves competitive

TABLE VIII
DOMAIN- AND CLASS-INCREMENTAL EXPERIMENTS. WE COMPARE WITH THE STATE-OF-THE-ART ON DN4IL, A BALANCED SUBSET OF DOMAINNET FOR INCREMENTAL LEARNING [32].

		Cold Start	
		A_{step}^K	A_{inc}^K
Method		6 Step	6 Step
DN4IL	EWC	9.81 ± 0.47	25.55 ± 0.23
	LwF	10.50 ± 0.89	27.86 ± 0.56
	PASS	24.44 ± 0.19	37.14 ± 0.10
	FeTrIL	30.95 ± 0.17	40.39 ± 0.11
	SSRE	32.05 ± 0.09	41.25 ± 0.18
	FeCAM	36.42 ± 0.12	42.93 ± 0.11
	R-DFCIL	22.31 ± 0.21	32.18 ± 0.29
	EFC	38.27 ± 0.16	45.85 ± 0.25
	EFC++	39.32 ± 0.15	46.20 ± 0.21

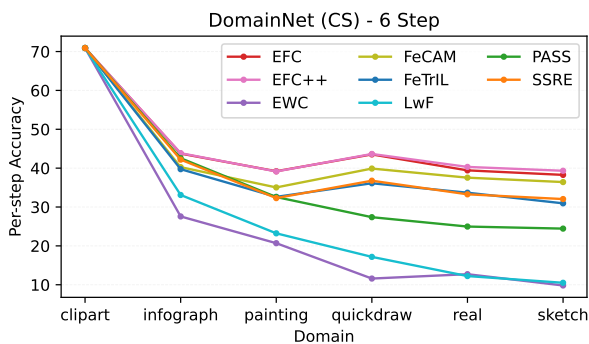


Fig. 14. Per-step accuracy during the incremental learning on DN4IL. We compare EFC++ with the state-of-the-art in a setting in which each incremental learning step represents a different domain.

performance, though it still falls short of the state-of-the-art. In Figure 14, we show the per-step accuracy across all encountered domains.

APPENDIX G

VALIDATION ON REGULARIZATION HYPERPARAMETERS

In this section, we present the results of the same analysis as Figure 11 in the main paper but for different scenarios on CIFAR-100. The grid search is performed over $\lambda_{\text{EFM}} \in \{1, 5, 10, 50, 100\}$ and damping $\eta \in \{10^{-3}, 10^{-2}, 10^{-1}, 1, 10\}$. Figure 15 shows that the selected combination ($\lambda_{\text{EFM}} = 10$ and $\eta = 0.1$) exhibits a *very good trade-off between stability and plasticity across all tested scenarios*. However, at the cost of an expensive search, we found that slightly better combinations exist for specific setting, e.g., changing λ_{EFM} to 5 for a 20-step Cold Start or $\eta = 1$ for a 20-step Warm Start.

APPENDIX H

ABLATION ON EFM REGULARIZER

In Section VIII-A of the main paper, we discuss what happens when we substitute EFM with three established regularizers: the Fisher Information Matrix (E-FIM, Eq. 3 main), Feature Distillation (FD, Eq. 5 main), and Knowledge Distillation (KD). Here, we expand that discussion by providing more details on the choice of hyperparameters We recall

TABLE IX
IMPACT OF MEAN AND COVARIANCE DRIFT ON EFC++ TESTED ON IMAGENET-SUBSET CS.

Step	Mean	Covariance	Accuracy	Delta
10	Fixed	Fixed	52.95 ± 1.00	—
	EFM	Fixed	53.90 ± 1.18	+0.95
	EFM	Real	52.44 ± 1.21	-0.51
	Real	Fixed	56.14 ± 1.04	+3.19
	Real	Real	55.69 ± 1.13	+2.74
20	Fixed	Fixed	39.10 ± 0.86	—
	EFM	Fixed	40.86 ± 1.65	+1.76
	EFM	Real	41.84 ± 1.30	+2.74
	Real	Fixed	49.70 ± 1.09	+10.60
	Real	Real	50.12 ± 1.42	+11.02

that the *only* modification to our training framework in this analysis concerns the regularization loss. The prototype update, which requires the EFM matrix, and the rebalancing of the classifier after training the backbone on the new classifier remain unchanged.

For this analysis, we validate the hyperparameters for each regularizer: $\lambda_{\text{E-FIM}} \in \{100, 500, 5000, 10000, 100000\}$, $\lambda_{\text{KD}} \in \{1, 5, 10, 50, 100\}$, and $\lambda_{\text{FD}} \in \{0.1, 1, 5, 10, 50, 100\}$. Unlike EFM, where we have a theoretical explanation for the choice of hyperparameters (see Section VIII-C in the main paper), here we lack guidance on optimal values. Thus, in Table IV of the main paper we report the results obtained with the hyperparameters that perform best in each setting. Looking at the final per-step accuracy, we found that the best trade-off across settings is achieved with $\lambda_{\text{E-FIM}} = 100, 000$, $\lambda_{\text{KD}} = 50$, and $\lambda_{\text{FD}} = 1$.

APPENDIX I

COVARIANCE DRIFT

This section extend the discussion in Section VIII-E on the limitations of prototype rehearsal in EFC++ illustrating the results obtained on Tiny-ImageNet and on ImageNet-Subset CS. In particular, Table X and Table IX compare different update strategies of class statistics: our approach (class means estimated via EFM and fixed covariances, highlighted in cyan) against an idealized upper bound using real mean and covariances.

APPENDIX J

PER-STEP ACCURACY PLOTS

A. Warm Start Scenarios

In Figure 16 we compare the per-step incremental accuracy of EFC++ with recent approaches in Warm Start across all three datasets for various task sequences. All methods begin from the same starting point after training on the large first task. EFC++ obtains significantly better results compared to FeCAM, in the 10-step scenario and achieves comparable results in the longest scenario. Thanks to the Prototype Re-balancing phase, EFC++ achieves a better stability-plasticity tradeoff compared to EFC, consistently resulting in superior performance.

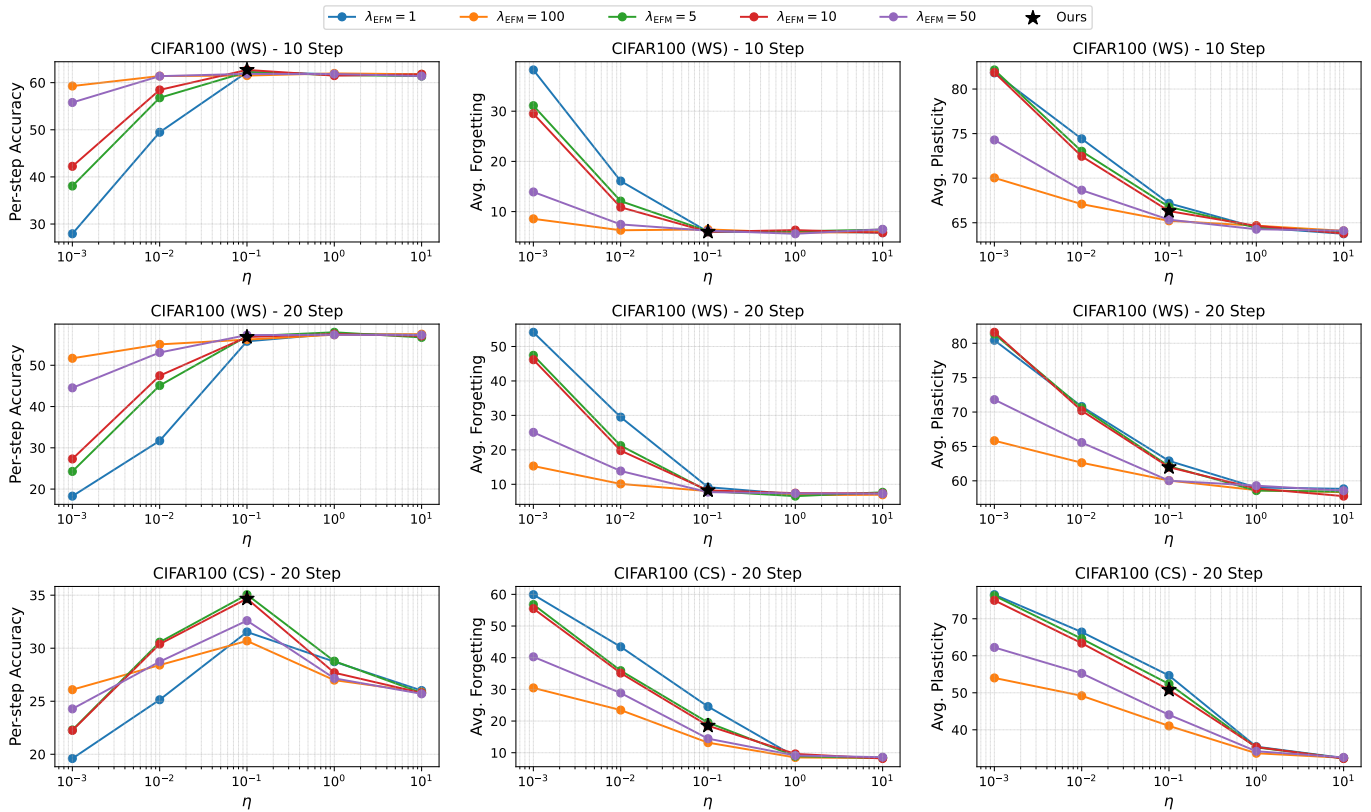


Fig. 15. A grid search testing 25 combinations of λ_{EFM} , with the x -axis in log scale for better visualization. The y -axes represent per-step accuracy, average plasticity, and average plasticity after the final step.

TABLE X
IMPACT OF MEAN AND COVARIANCE DRIFT ON EFC++ TESTED ON TINY-IMAGENET CS.

Step	Mean	Covariance	Accuracy	Delta
10	Fixed	Fixed	36.17 ± 0.48	—
	EFM	Fixed	37.48 ± 0.52	+1.31
	EFM	Real	37.47 ± 0.27	+1.30
	Real	Fixed	39.94 ± 0.43	+3.77
	Real	Real	39.95 ± 0.55	+3.78
20	Fixed	Fixed	29.04 ± 0.65	—
	EFM	Fixed	32.56 ± 0.44	+3.52
	EFM	Real	31.89 ± 0.10	+2.85
	Real	Fixed	36.30 ± 0.31	+7.25
	Real	Real	37.00 ± 0.12	+7.96

B. Cold Start Scenarios

In Figure 17 we compare the per-step incremental accuracy of EFC++ with recent approaches in Cold Start across all three datasets for various task sequences. All methods begin from the same starting point after training on the small first task, but EFC++ (and EFC), enhancing plasticity thanks to the EFM regularizer, outperform state-of-the-art competitors. Thanks to the Prototype Re-balancing phase, EFC++ achieves a better stability-plasticity tradeoff compared to EFC, consistently resulting in superior performance.

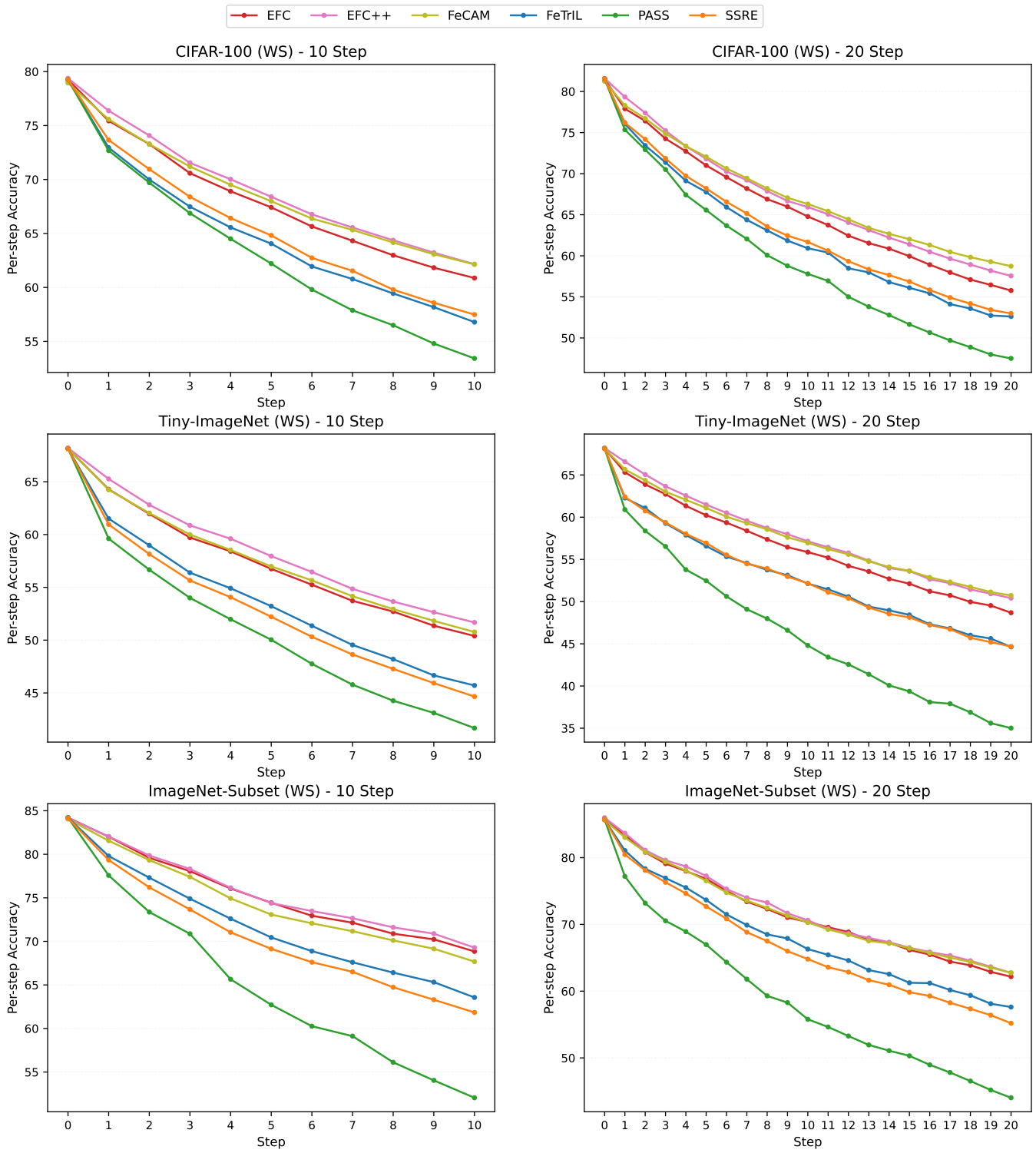


Fig. 16. Warm Start (WS) per-step accuracy during the incremental learning. The plots compare recent EFCIL methods against EFC++ on three different dataset for different incremental step sequences.

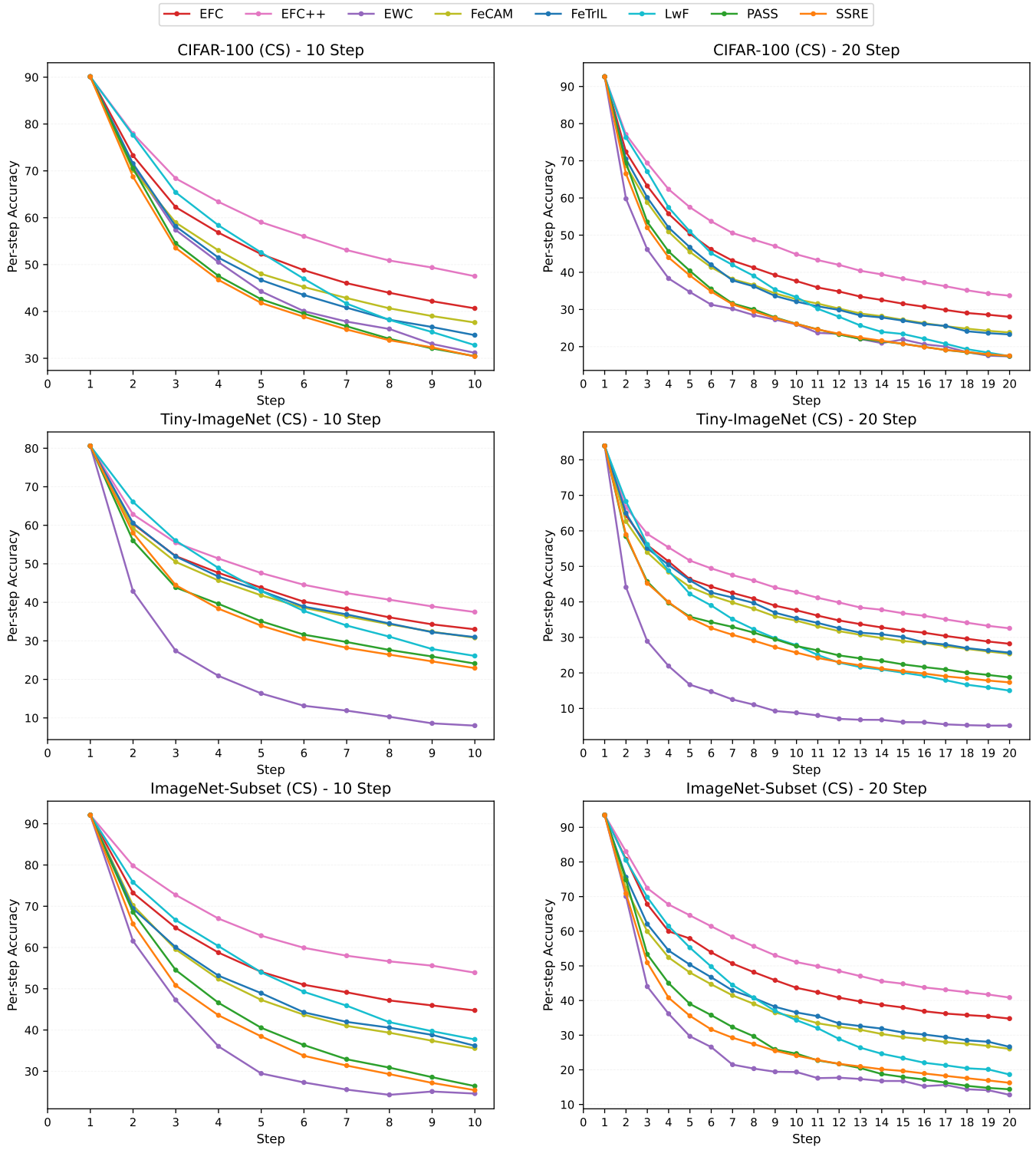


Fig. 17. Cold Start (CS) per-step accuracy plots during incremental learning. The plots compare recent EFCIL methods with EFC++ on three different datasets for different incremental step sequences.